Stability and Antimicrobial Activity of Nisin-Loaded Mesoporous Silica Nanoparticles: A Game-Changer in the War against Maleficent Microbes

Behzadi, Faezeh; Darouie, Sheyda; Alavi, S. Mehdi; Shariati, Parvin; Singh, Gurvinder; Dolatshahi-Pirouz, Alireza; Arpanaei, Ayyoob

Published in:
Journal of Agricultural and Food Chemistry

Link to article, DOI:
10.1021/acs.jafc.7b05492

Publication date:
2018

Document Version
Peer reviewed version

Food Safety and Toxicology

The stability and antimicrobial activity of nisin-loaded mesoporous silica nanoparticles: A game-changer in the war against maleficent microbes

Faezeh Behzadi, Sheyda Darouie, Seyed Mehdi Alavi, Parvin Shariati, Gurvinder Singh, Alireza Dolatshahi-Pirouz, and Ayyoob Arpanaei

J. Agric. Food Chem., **Just Accepted Manuscript** • DOI: 10.1021/acs.jafc.7b05492 • Publication Date (Web): 05 Apr 2018

The stability and antimicrobial activity of nisin-loaded mesoporous silica nanoparticles: A game-changer in the war against maleficent microbes

Faezeh Behzadi[a], *Sheyda Darouie*[a], *S. Mehdi Alavi*[b], *Parvin Shariati*[a], *Gurvinder Singh*[c], *Alireza Dolatshahi-Pirouz*[d] *and Ayyoob Arpanaei*[a,*]

[a] Department of Industrial and Environmental Biotechnology, National Institute of Genetic Engineering and Biotechnology (NIGEB), Shahrak-e Pajoohesh, km 15, Tehran - Karaj Highway, Tehran, Iran.

[b] Department of Agricultural Biotechnology, National Institute of Genetic Engineering and Biotechnology (NIGEB), Shahrak-e Pajoohesh, km 15, Tehran - Karaj Highway, Tehran, Iran.

[c] Department of Materials Science and Engineering, Norwegian University of Science and Technology, Trondheim-7491, Norway.

[d] Center for Nanomedicine and Theranostics, DTU Nanotech, Technical University of Denmark, Kgs Ørsteds Plads, 2800-Kongens Lyngby, Denmark.

[*] **Corresponding Author**

Ayyoob Arpanaei, E-mail: arpanaei@yahoo.com, aa@nigeb.ac.ir; Tel: +98 21 44787463, Fax: +98 21 44787395

ABSTRACT: Antimicrobial agents, such as nisin are used extensively in the food industry. Here, we investigated various approaches to load nisin onto mesoporous silica nanoparticles (MSNs, 92 ± 10 nm in diameter), so as to enhance its stability and sustained release. The morphology, size and surface charge of the as-prepared nanoparticles were analyzed using STEM, DLS and ζ (zeta) potential measurement. Nisin was either physically adsorbed or covalently attached to the variously functionalized MSNs, with high loading capacities (>600 mg nisin g^{-1} nanoparticles). The results of antibacterial activity analysis nisin against *Staphylococcus aureus* showed that despite of very low antibacterial activity of the nisin covalently conjugated onto MSNs, the physical adsorption of nisin onto the unfunctionalized nanoparticles enhances its antimicrobial activities under various conditions, with no significant cytotoxicity effects on mouse fibroblast L929 cells. In conclusion, MSNs can be recommended as suitable carriers for nisin under various conditions.

KEYWORDS: Antimicrobial property, nisin, mesoporous silica nanoparticle, loading approach, foodborne pathogen

1. Introduction

Various antimicrobial compounds are currently being used to prevent microbial contamination of food and other nutrient-containing systems [1,2]. Nisin, a small peptide with a molecular weight of 3.5 kDa, is naturally produced by *Lactococcus lactis* strains and has been broadly used as a natural antimicrobial food preservation material. A positively charged amphiphilic bacteriocin at neutral pH, this peptide is very effective in inhibiting the growth of Gram-positive, spore-forming spoilage and pathogenic bacteria, such as *Staphylococcus aureus* [3,4]. The antibacterial properties of nisin is related to its ability of binding to the negatively charged cytoplasmic membranes of target cells, thus resulting in pore formation. This leads to the efflux of small essential cytoplasmic substances from the target cells [5–8]. The major challenge in the use of nisin as a natural preservation is its rapid depletion after initial application. In fact, the stability and antimicrobial activity of nisin are reduced by several intrinsic and extrinsic environmental factors, such as heat treatments at high temperatures, storage at alkaline pH, long processing times and interaction of the peptide with the food matrix during processing and storage stages [9–11]. In addition, overuse and misuse of antibiotics is the main reason for the antibiotics resistant pathogens. This issue has become one of the biggest threats to global health. Development of novel methods for the formulation of antibiotics may be one of the solutions to overcome this problem [12]. To address these problems, the development of a delivery system to improve the stability and the efficacy of antimicrobial agents, such as nisin as a food antimicrobial agent, can be considered as an efficient approach.

Recently, the application of nanomaterials has received significant attention in the food industry due to their physicochemical characteristics as delivery systems of various compounds including food antimicrobial agents [13,14]. The results of recent studies have shown that the

63 loading of nisin onto nanoparticles makes its controlled release feasible and may increase its
64 stability and bioactivity [15–21]. Among the wide selection of nanomaterials, mesoporous silica
65 nanoparticles (MSNs) have recently become the focus of many investigations as carriers of
66 different types of biomolecules. These nanoparticles present unique physicochemical
67 characteristics, such as a large surface area, size controllability, easy functionalization, thermal
68 stability, as well as excellent biocompatibility and biodegradability [22–26]. Furthermore, the studies
69 demonstrate that immobilization of antimicrobials onto MSNs can enhance their antimicrobial
70 effects and improve their stability [25,27–29]. Despite the properties and enormous applications of
71 MSNs, their ability to load nisin has not been studied so far. Thus, the focus of the present work
72 is to design and investigate a suitable carrier for the delivery of nisin based on unfunctionalized
73 or chemically-functionalized MSNs. In this regard, MSNs of various surface chemistries were
74 prepared and then, then was used for the loading of nisin via either physical adsorption or
75 covalent attachment approaches under various conditions. Subsequently, the stability and
76 bioactivity of nisin-loaded particles and the free nisin against the *Staphylococcus aureus* (ATCC:
77 6538) bacterium, were evaluated under various conditions by measuring the minimal inhibition
78 concentration (MIC) of the as-prepared samples. In addition, *in vitro* cytotoxicity of the as-
79 prepared antimicrobial systems was investigated using the MTT assay. To the best of our
80 knowledge, this is the first report on the application of MSNs as a biocompatible carrier for
81 loading nisin and study of the antibacterial activity and stability of the nisin-loaded MSNs.

82 **2. Materials and methods**

83 **2.1. Materials**

Nisin (as the Nisaplin form containing 2.5% (w/w) of nisin), N-hydroxysuccinimide (NHS) and N-(3-dimethylaminopropyl)-N-ethylcarbodiimide hydrochloride (EDC) were obtained from Sigma-Aldrich (St. Louis, MO, USA). Tetraethylorthosilicate (TEOS), cetyltrimethylammonium bromide (CTAB), [3-(2-aminoethylamino)propyl]trimethoxysilane (EDS, 97% v/v), dimethylformamide (DMF), succinic anhydride, polyethyleneimine (PEI, M.W. 10000) and brain-heart infusion (BHI) were purchased from Merck (Darmstadt, Germany). Dulbecco's modified Eagle's medium (DMEM) was acquired from STEMCELL Technologies Inc. (Vancouver, Canada). Fetal bovine serum (FBS) was purchased from Invitrogen (Carlsbad, California, USA). Water was deionized using the Q-check controller system (OES Co., USA).

2.2. Synthesis and surface modification of MSNs

The MSNs were prepared and functionalized according to a previously reported approach based on the template removing method [30]. In brief, 100 mg of CTAB and 350 μL of sodium hydroxide aqueous solution (2 M) were added to 48.65 mL of water at 80 ^{o}C with constant stirring. Then, 1 mL of TEOS was added in a dropwise manner and the mixture was stirred for 2 h. To remove CTAB, the resulting bare MSNs (BMSNs) were then dispersed in an acidic solution of ethanol with an HCl: ethanol ratio of 1:10 (v/v) and refluxed at least twice for 3 h.

To prepare amine-, carboxyl-, and PEI-coated MSNs (AMSNs, CMSNs, and PAMSNs, respectively), EDS, succinic anhydride, and PEI were used, respectively. For the preparation of AMSNs, 200 mg of the as-prepared BMSNs was dispersed in absolute ethanol (4.6 mL). Deionized water (200 μL), acetic acid (100 μL), and EDS (100 μL) were then added and the mixture was allowed to react for 1 h at room temperature. In order to synthesize CMSNs, AMSNs were used. For this purpose, 100 mg of AMSNs was re-dispersed in DMF (20 mL), and

106 200 mg of succinic anhydride was subsequently added. The mixture was stirred at room
107 temperature under a nitrogen atmosphere overnight. In order to prepare PEI-coated MSNs
108 (PAMSNs), 100 mg of CMSNs were first dispersed in phosphate buffered saline (PBS) (10 mM,
109 pH 7.4) containing NHS (0.2 mg mL^{-1}) and EDC (1 mg mL^{-1}). The obtained suspension was
110 shaken for 8 min and then centrifuged at 2380×g for 3 min. Subsequently, 10 mL of PEI
111 solution (2 mg mL^{-1}) was added to the suspension and the mixture was shaken for 1 h. Finally,
112 the mixture was centrifuged at 2380×g for 10 min and the synthesized PAMSNs washed three
113 times with PBS.

114 **2.3. Characterization of nanoparticles**

115 The size and morphology of MSNs were studied by scanning transmission electron
116 microscopy (STEM) using a HITACHI S5500 electron microscope operating at 30 kV.
117 Furthermore, the Malvern Zetasizer Nano instrument (S90, UK) equipped with the dynamic light
118 scattering (DLS) system was used to measure zeta potential values and hydrodynamic diameters
119 of the MSNs, respectively.

120 **2.4. Nisin physical adsorption, covalent conjugation and release studies**

121 To study the physical adsorption of nisin onto BMSNs and CMSNs, various amounts of nisin
122 (35, 50, 100, 200, and 400 μg) were added to the as-prepared nanoparticles (200 μg of each MSN
123 in 750 μL of sodium acetate buffer, 50 mM, pH 5.5). The samples were incubated at room
124 temperature on an orbital shaker, shaking at 60 oscillations min^{-1} for 2 h. For the covalent
125 immobilization of nisin onto AMSNs and PAMSNs, 100 μL of glutaraldehyde (25% v/v) was
126 added to the particle suspensions (200 μg of AMSNs or PAMSNs in 750 μL of sodium acetate
127 buffer, 50 mM, pH 5.5) and the resulting suspension was then shaken for 1 h. Thereafter, the

samples were washed with sodium acetate buffer (50 mM, pH 5.5) and subsequently, nisin (35, 50, 100, 200, and 400 μg) was quickly added to the suspensions. The reaction was allowed to proceed with shaking at 60 oscillations min^{-1}, overnight. For the covalent conjugation of nisin to CMSNs, an EDC (10.43 mM) /NHS (3.48 mM) solution in acetate buffer (50 mM, pH 5.5) was added to the CMSNs suspension (5 mg in 2.5 mL buffer) and the resulting mixture was allowed to shake for 10 min using a rocking chair. Nisin (35, 50, 100, 200, and 400 μg) was quickly added to the activated CMSNs suspension and the reaction was allowed to proceed with shaking (60 oscillations min^{-1}) for 2 h. In all loading tests, after completion of the reaction, free nisin was removed by triplicate washings using an acetate buffer solution and centrifugation at 16000×g for 15 min. The amount of loaded nisin was determined by measuring residual nisin in the solution using the Bradford assay with a T80+UV/Vis spectrophotometer (PG instruments Ltd, UK). To obtain the final amount of loaded nisin, the residual nisin level was subtracted from the initial amount of nisin used in the loading process. To confirm the above results, high performance liquid chromatography (HPLC) technique (Cecil Instruments, UK) at a wavelength of 225 nm was employed for a limited number of samples (200 μg nisin: 200 μg MSNs). HPLC tests were performed in duplicate. Nisin loading capacities (LC) and loading efficiencies (LE) were estimated using equations 2.1 and 2.2, respectively, as follows:

$$\mathrm{LC}\left(\frac{\mathrm{mg}}{\mathrm{g}}\right) = \frac{\text{Mass of loaded nisin (mg)}}{\text{Mass of applied MSNs (g)}} \qquad \text{(Equation 2.1)}$$

$$\mathrm{LE}\ (\%) = \frac{\text{Mass of loaded nisin (mg)}}{\text{Total mass of applied nisin (mg)}} \times 100 \qquad \text{(Equation 2.2)}$$

Nisin adsorption isotherms for unfunctionalized and CMSNs were obtained using adsorption tests described in the previous section. To study the kinetic parameters of the adsorption process,

147 Langmuir, Freundlich, and Langmuir-Freundlich models [31,32] (equations 2.3, 2.4 and 2.5,
148 respectively) were employed.

$$q_e = \frac{q_m C_e}{K_l + C_e} \quad \text{(Equation 2.3)}$$

$$q_e = K_F C_e^{1/n} \quad \text{(Equation 2.4)}$$

149 $$q_e = \frac{q_m K_c C_e^{1/n}}{1 + K_c C_e^{1/n}} \quad \text{(Equation 2.5)}$$

150 In order to investigate the nisin desorption kinetics, nisin-loaded MSNs were dispersed in
151 acetate (50 mM, pH 5.5), phosphate (50 mM, pH 7.5) or Tris (50 mM, pH 9.5) buffers and then
152 shaken at 180 oscillations min^{-1} in an incubator at 37 °C (conditions under which the bacterial
153 growth is supported) for 120 h. After centrifugation (16000×g, 15 min), the released nisin
154 present in the supernatant was measured at various time intervals. The zero-order, first-order and
155 the power-law models [33,34] (equations 2.6, 2.7 and 2.8, respectively) were used to describe the
156 release profile of the loaded nisin.

$$\frac{M_t}{M\infty} = 1 - e^{(-klt)} \quad \text{(Equations 2.6)}$$

$$\frac{M_t}{M\infty} = K_0 t \quad \text{(Equations 2.7)}$$

157 $$\frac{M_t}{M\infty} = Kt^n \quad \text{(Equations 2.8)}$$

158 The stability of the nisin conjugated to AMSNs, PAMSNs, and CMSNs was also studied in
159 phosphate buffer (50 mM, pH 7.5). Accordingly, nisin-conjugated samples were dispersed in the
160 buffer and centrifuged at regular time intervals. The obtained supernatant was used to measure

161 the amount of released nisin. In this section, all experiments were repeated at least three times in
162 parallel.

163 **2.5. Antimicrobial activity studies**

164 MIC was used to determine nisin's bacteriostatic activity via individual incubations of 1×10^6
165 CFU mL^{-1} *Staphylococcus aureus* (ATCC: 6538) in BHI medium at 37 ^oC for 18 h, in the
166 presence of the free nisin, nisin-physically adsorbed BMSNs (nisin+BMSNs), nisin-physically
167 adsorbed CMSNs (nisin+CMSNs), nisin-conjugated CMSNs (nisin-CMSNs), nisin-conjugated
168 AMSNs (nisin-AMSNs) or nisin-conjugated PAMSNs (nisin-PAMSNs), at seven nisin
169 concentration levels (12.5, 18.5, 25, 37.5, 50, 62.5 and 75 μg mL^{-1}). The bacterial cell viability
170 was determined spectrophotometrically by measuring optical density (OD) at a wavelength of
171 620 nm using an ELISA plate reader (System Multidkan Titertek Lab MS., Netherland). All
172 experiments were repeated at least three times in parallel.

173 **2.6. Evaluation of cytotoxicity effects of bare, carboxylated and nisin-loaded MSNs**

174 The *in vitro* cytotoxic effects of bare and carboxylated MSNPs, free nisin and nisin-loaded
175 MSNs on the mouse fibroblast L929 cell line was tested using the MTT assay. Accordingly,
176 mouse fibroblast cells were cultured in DMEM containing 10% FBS, 100 μg mL^{-1} streptomycin,
177 and 1.00 U mL^{-1} penicillin at 37 ^oC in a humidified atmosphere (90%) with 5% CO_2. In each
178 well of a 96-well plate, 7000 cells were seeded into 100 μL of medium. After 24 h, the cells were
179 treated with solutions containing BMSNs, CMSNs, and nisin at concentrations of 125, 250, 500
180 or 1000 μg mL^{-1}. The cells were also treated with 10, 25, 50, 100 or 200 μg mL^{-1} of nisin
181 physically adsorbed onto BMSNs and CMSNs (nisin+BMSNs and nisin+CMSNs, respectively).
182 After another 24 h, 10 μL of the MTT reagent (5 mg mL^{-1} in PBS) was added to each well, and

183 the plate was incubated for a further 4 h. Eventually, 100 mL of DMSO was added to each well
184 and the OD was measured at 580 nm using the ELISA plate reader. The results were then
185 reported as the cell viability percentage by using equation 2.9:

$$\text{Cell viability [\%]} = \frac{\text{OD of treated cells}}{\text{OD of untreated cells (control)}} \times 100 \qquad \text{(Equation 2.9)}$$

186 **3. Results and discussion**

187 **3.1. Characterization of MSNs**

188 The size and morphology of the MSNs were examined by STEM and DLS methods. STEM
189 images reveal the spherical morphology of the as-prepared MSNs with an average diameter of
190 approximately 92 ±10 nm (Figure 1). However, the mean diameter of MSNs measured by the
191 DLS technique is slightly larger (~113 nm) than that determined by the STEM procedure. This is
192 due to the fact that DLS analysis measures the hydrodynamic size of the particles, which is
193 usually larger than the actual size of the particles. The mean pore diameter and specific surface
194 area as measured in our previous studies [27,30,35], are 4.1 nm and 882.1 m^2 g^{-1}, respectively. In
195 those works, it was shown that the as-prepared MSNs present a structure of MCM-41 [27,30,35],
196 which have channel-like pores [26]. For small molecules like nisin with a molecular weight of 3.5
197 kDa [3,4], this pore diameter is appropriate for the mass transfer into the pores. It might also be
198 noted that 4.1 nm is the average size of the pore diameters, which means that the existence of
199 pores with larger diameters facilitate the nisin adsorption. On the other hand, owing to the high
200 specific surface area of the as-prepared nanoparticles, large values of loading capacity for nisin
201 are also expected.

The surface functionalization of MSN samples was evaluated by zeta (ζ) potential measurements of particles in deionized water. The results obtained imply that surface functionalization of the nanoparticles was achieved successfully. While the surface charge of the unfunctionalized BMSNs was approximately -28 mV, the ζ potential values of AMSNs, CMSNs, and PAMSNs were found to be approximately +11, -40 and +24 mV, respectively. These results demonstrate that amine-functionalized MSNs (AMSNs) possess positively charged surfaces, whereas carboxyl-functionalized MSNs (CMSNs) have more negatively charged surfaces in comparison to that of the BMSNs. Correspondingly, the functionalization of MSNs with PEI molecules leads to more positively charged surfaces, owing to the presence of a high number of primary, secondary and tertiary amine groups in the PEI molecules.

3.2. Physical adsorption and covalent conjugation of nisin to MSN samples

In this work, different approaches, including physical adsorption onto BMSNs and CMSNs and covalent conjugation to AMSNs, PAMSNs, and CMSNs, were applied to load nisin onto MSNs. The scheme 1 presents a schematic illustration of the applied methods [36–38]. Due to a higher solubility and stability of nisin in acidic buffers, sodium acetate buffer (50 mM, pH 5.5) was selected for the loading procedure to ensure minimized loss of antibacterial activity. Under this condition, nisin exhibits a positive charge due to its basic isoelectric point (8.5). It is expected that nisin can electrostatically adsorb onto the surface of BMSNs and CMSNs with negatively charged surfaces. Therefore, nisin physically adsorbed onto BMSN and CMSN samples (nisin+BMSNs and nisin+CMSNs, respectively) were prepared.

To study the kinetics of nisin adsorption onto BMSNs and CMSNs, adsorption isotherm curves were obtained (Figure 2). Data obtained for nisin adsorption onto BMSNs and CMSNs were

fitted into Langmuir, Freundlich and Langmuir-Freundlich models. As it can be seen in Figure 2, among these three models, the Langmuir-Freundlich model appropriately fits nisin adsorption onto both negatively charged MSNs. The obtained values for the equation's parameters are presented in Table 1.

The Langmuir-Freundlich model relies on the fact that the adsorption surface is heterogeneous [31,32]. One hypothesis to describe the adsorption mechanism for the current process can be that the absorbent's surface is homogeneous at the beginning of the adsorption process. But as adsorption continues the interaction between amphiphilic nisin molecules makes the surface heterogeneous and multilayers of adsorbed nisin molecules are eventually formed. Very high values of the maximum loading capacities, q_m, for nisin adsorption onto BMSNs and CMSNs (Table 1) obtained in the current study can support the abovementioned hypothesis.

As shown in Figure 2, the adsorption of nisin onto MSNs increases and the loading efficiency decreases when increasing the initial concentration of the applied nisin. Reduced loading efficiency levels of unfunctionalized MSNs (BMSNs) as obtained by increasing initial nisin concentrations, is higher than that of the CMSNs, which is likely due to the lower BMSNs' surface charge values.

To have the maximum and advantageous loading capacity, an initial nisin concentration of 0.267 μg mL^{-1} (200 μg of nisin in 750 μL of acetate buffer) was chosen for the release studies. The results of the release studies are presented in the next section. At this point, the nisin-loading capacities of the BMSNs and CMSNs were calculated to be 624.6 and 701.3 mg nisin g^{-1} MSNs, and the loading efficiency values were found to be 62.46 and 70.13%, respectively. These nisin loading efficiency values were comparable to other studies by Bi et al. [39], Prombutara et al. [40] and

Zou et al. [41] who reported 62.5%, 73.6% and 70.3% loading efficiencies of nisin onto liposomal, carbohydrate and solid lipid nanoparticles, respectively.

In the case of positively charged nanoparticles, *i.e.* AMSNs and PAMSNs, the efficiency of physical nisin adsorption was expected to be low, since the net charges of nisin and the nanoparticles are both positive at the applied pH (5.5). Our obtained results confirmed this, since the adsorption of nisin onto AMSNs and PAMSNs was very low, as it was expected (data not shown).

In another approach, nisin was attached covalently to the positively charged nanoparticles containing amine groups using glutaraldehyde to prepare nisin-covalently conjugated-AMSN and PAMSN samples (nisin-AMSNs and nisin-PAMSNs, respectively). Finally, to prepare the nisin-CMSNs sample, the carboxyl groups of the CMSNs were activated with an EDC/NHS mixture and used for the covalent binding of nisin through its amine groups to the carboxyl groups of these nanoparticles. Figure 3 shows the capacity and efficiency of nisin conjugation to these three MSNs. The nisin-loading capacity increases and the loading efficiency decreases by increasing the initial nisin concentration for the three samples. The results obtained show that the higher nisin loading capacities and efficiencies can be achieved for the CMSNs relative to those for the AMSNs and PAMSNs, by covalent conjugation of nisin at high concentrations of this peptide ($\geq$0.267 μg mL^{-1}). The nisin-loading capacity for PAMSNs is less than that for the AMSNs and CMSNs. This could be due to the existence of attractive electrostatic forces between negatively charged CMSNs and positively charged nisin molecules, and electrostatic repulsion forces between the highly positively charged nanoparticles (PAMSNs) and positively charged nisin peptide molecules, under the applied conditions. These data indicate that even for the covalent conjugation of molecules to particle surfaces, electrostatic interactions can play a

269 significant role in facilitating or hampering the adsorbate molecules approaching the binding
270 sites on the nanoparticle's surface. Consequently, this can enhance or diminish the conjugation
271 process, depending on the type of electrostatic interaction.

272 As an alternative assessment method, the loading capacities of MSNs were also determined
273 using the HPLC technique. The HPLC data were in agreement with the results of the Bradford
274 protein assay (Figure 4).

275 **3.3. Nisin release from MSNs**

276 The nisin release studies were conducted in different buffers to evaluate the effects of various
277 pH values and buffers on the release profile and kinetics. Figure 5 exhibits the release isotherm
278 of nisin-loaded BMSNs and CMSNs, after 120 h of incubation in acetate (pH 5.5), phosphate
279 (pH 7.5) and Tris (pH 9.5) buffers. The results showed a high rate of nisin release during the first
280 24 h, which gradually decreased thereafter. The maximum nisin release values obtained for
281 nisin-BMSNs in acetate, phosphate and Tris buffers were 62.75, 92.96 and 96.36 %, while they
282 were 45.78, 70 and 100% for the nisin-loaded CMSNs, respectively, during a 120 h time-period.
283 *In vitro* release studies revealed that the highest and lowest release rates occurred in Tris and
284 acetate buffers, respectively. The high values for nisin release rates in Tris buffer (pH 9.5) can be
285 attributed to the anionic nature of nisin (pI 8.5) at high pH values, which renders its surface
286 negatively charged under such condition. Therefore, the negatively charged nisin molecules can
287 easily be released from the surface of negatively charges surfaces such as BMSNs and CMSNs,
288 in Tris buffer. In fact, the nisin release value for the CMSNs in Tris buffer is higher because of
289 being more negatively charged when compared to the BMSNs, according to their ζ potential
290 values (-28 and -40 mV for BMSNs and CMSNs, respectively). In contrast, the slower rate of
291 nisin release from the MSNs was obtained in acetate buffer due to this fact that nisin is higher

positively charged at pH 5.5 as compared to that at pH 7.5 (for phosphate buffer) and 9.5 (for Tris buffer). In the same way, the higher negative charges for CMSNs when compared to BMSNs, leads to slower rates of nisin release from the former, in acetate buffer. These results show that the most important interactions between MSNs and nisin are electrostatic interactions which control the adsorption capacities as well as the release profiles. However, other types of interactions such as van der Waals or hydrogen binding might also play roles in such a system.

Desorption kinetics were also studied in the abovementioned three buffers using three models, *i.e.,* the zero-order, first-order and the power-law models. Results showed that the best fit for the experimental data was obtained with the power-law model (Figure 6). In the power-law model, the type of the release mechanism depends on the value of n. For spherical particles, $n \leq 0.43$ corresponds to a Fickian diffusion mechanism and $0.43<n<0.85$, $n = 0.85$ and $n>0.85$ correspond to non-Fickian transport, Case II transport and Super Case II transport mechanisms, respectively [33,34]. Therefore, according to the release parameters (Table 2), Fickian diffusion could be the dominant release mechanism for nisin from both BMSNs and CMSNs in acetate, phosphate and Tris buffers. The main reason for this similarity between nisin-release mechanisms for both types of nanoparticles can be due to the similar interaction mechanisms between nisin and functional groups existing on both types of negatively charged MSNs (BMSNs and CMSNs), *i.e.* electrostatic interactions. Furthermore, the pore structure of MSNs is not expected to be significantly changed when the surface is functionalized with the very small EDS and SA molecules.

The release profiles of covalently conjugated-nisin from CMSNs, AMSNs and PAMSNs were studied in phosphate buffer (pH 7.5) at 37 °C. Small portions of nisin (2%, 5% and 15.5% for CMSNs, AMSNs and PAMSNs, respectively) are released in the first 16 hours which can be

attributed to the nisin molecules physically adsorbed on the surface of MSNs. However, the main part of the loaded nisin (98%, 95% and 84.5% for CMSNs, AMSNs and PAMSNs, respectively) remains on the nanoparticles, even after 128 hours, indicating its covalent conjugation to the nanoparticles. Furthermore, continued release of nisin for PAMSNs can be due to the isolation of parts of the PEI polymers coated on the PAMSNs during the release period, while the samples are shaken at 180 rpm. These results also show that the covalently attached peptides are more stable than the physically adsorbed ones, as expected (Figure 7 *vs* Figure 5).

3.4. Antibacterial activity of the nisin-loaded samples

In vitro antibacterial activity of loaded nisin was evaluated by monitoring the optical density of a bacterial suspension at 620 nm and measuring the MIC value of samples against *Staphylococcus aureus*. The results are presented in Figure 8. The initial assessment of the antibacterial activity of BMSNs, CMSNs, AMSNs, and PAMSNs indicated no activity for tested MSNs (data not shown). Results revealed that the covalent conjugation of nisin to CMSNs, AMSNs, and PAMSNs considerably restricts the antibacterial activity of the peptide regardless of the type of MSNs and the applied conjugation approach. This may be due to the restriction of peptide conformation and the subsequent loss of their activity (Figure 8).

According to Figure 8, the MIC values of the free nisin and nisin+BMSNs toward *S. aureus* were found to be 75 and 62.5 μg mL^{-1}, respectively. Nisin+CMSNs also reduced bacterial growth to some extent, but less than those for the free nisin and nisin+BMSNs samples. This can be attributed to the fact that, at pH 7.5, after 24 h of incubation, only 47% of the adsorbed nisin is released from nisin+CMSNs, while this amount is 65% for nisin+BMSNs (Figure 5). In other words, a more stable attachment of nisin to CMSNs significantly decreases the rate of nisin release into the medium, thereby reducing the antibacterial activity of the nisin+CMSNs.

The results presented in Figure 8 also show that the controlled release of nisin from nisin+BMSNs enhances antibacterial efficiency and lowers the MIC value in comparison to that of the free nisin. In general, the slow release of adsorbed nisin from BMSNs and CMSNs can protect it against unfavorable reactions and consequently control its bioavailability, promote the stability and eventually augment its antibacterial effects under different conditions. Hence, in the next steps of this study, the antibacterial activity of nisin-loaded MSNs was evaluated by changing the preservation time under neutral pH as well as alkaline conditions. With respect to very low antimicrobial activities of the nisin-conjugated samples, *i.e.,* nisin-AMSNs, nisin-PAMSNs and nisin-CMSNs, they were not considered for further investigation in the next steps of this research.

The results presented in Figure 9 show that the antibacterial activity of the free nisin solutions at different concentrations drastically decreases when increasing the preservation time. After 72 h, the antibacterial activity of free nisin falls dramatically for all concentrations, gradually decreasing to about 20%, while in the case of nisin+BMSNs, the retained activity is about 50% of the initial activity after 120 h (Figure 9). The results obtained also revealed that the activity of nisin+CMSNs samples is much lower than that of the nisin+BMSNs; but, it is slightly higher than that for free nisin at high concentrations and preservation times longer than 72 h. This observation can be attributed to the fact that the interaction between CMSNs and the peptide is relatively stable even over long preservation periods, thus limiting its bioavailability and consequently its antibacterial activity. Since the ultimate goal of loading antimicrobial agents such as nisin, onto carriers, is an enhancement of stability and augmentation of antibacterial properties, these results reveal the prominent advantages of BMSNs and even CMSNs as valuable carriers for nisin and possibly other antimicrobial agents.

The effect of alkaline conditions on the antimicrobial activity of free nisin and nisin-loaded samples (nisin+BMSNs and nisin+CMSNs) was studied in Tris buffer, pH 9.5. Under this condition, the antibacterial activity of free nisin was reduced considerably in comparison to that at pH 7.5 (phosphate buffer). In contrary, the antibacterial activity of nisin adsorbed onto BMSNs and CMSNs significantly intensified at pH 9.5 (Figure 10). Under this condition, the MIC values of nisin+BMSNs and nisin+CMSNs toward *S. aureus* were 62.5 and 50 μg mL^{-1}, with the release rates of 67 and 80%, respectively. Since nisin's net charge is negative at pH 9.5, the rate of nisin release from CMSNs was higher than that of the BMSNs (because of a higher negative surface charge), as shown in Figure 5, leading to a higher value of antibacterial activity and consequently a lower MIC level for the former. In general, these results indicate that the physical adsorption of nisin onto negatively charged MSNs not only increases its stability but also enhances its antibacterial activity at alkaline pH.

3.5. Evaluation of the cytotoxicity of effects of MSNs and nisin-loaded MSNs

One of the challenges in using antimicrobial carriers is their cytotoxicity to mammalian cells. In this research, the cytotoxicity of these carriers was studied using the MTT assay. Figure 11a shows that the cell viability of mouse fibroblast L929 cells does not change considerably following an increase in MSNs concentration, even when it is as high as 1000 μg mL^{-1}. Only in the case of BMSNs, minor cytotoxic effects were observed (Figure 11a).

The cytotoxic effects of free nisin and nisin-loaded MSNs (nisin+BMSNs and nisin+CMSNs) were also studied. The results showed that free nisin has relatively non-toxic effects on the mouse fibroblast cells (Figure 11b). These results also revealed that the nisin-loaded BMSNs and

382 CMSNs do not inhibit the growth of the cells in all tested nisin concentrations (10-200 mg.mL^{-1})
383 (Figure 11b).

384 In general, the main aim of the current study is to develop an efficient method for the loading
385 of nisin onto mesoporous silica nanoparticles of various surface chemistries, so as to enhance the
386 antimicrobial agent's stability under various conditions. The obtained results in the current study
387 on the nisin when loaded on the nanoparticles are comparable to those reported in previous
388 studies [17,39–41]. The results obtained in those studies indicate that the loading of nisin onto
389 nanoparticles such as chitosan/alginate [17], liposomal [41], solid lipid [40] and carbohydrate
390 nanoparticles [39] improves its antibacterial activity and stability. However, in none of those
391 studies, the effect of the loading approach as well as applying an alkaline pH was investigated.
392 Generally, the loading approach of biomolecules onto nanoparticles can have a very fundamental
393 effect on their biological activity and stability [13,19]. The results obtained in this study revealed
394 that the physical adsorption of nisin onto negatively charged mesoporous silica nanoparticles,
395 *i.e.,* bare mesoporous silica nanoparticles and carboxyl-functionalized mesoporous silica
396 nanoparticles, or its chemical conjugation to amine-functionalized, polyethyleneimine-coated
397 and carboxyl-functionalized mesoporous silica nanoparticles can be achieved with high loading
398 capacities and efficiencies. However, the antimicrobial activity of the loaded nisin strikingly
399 depends on the loading approach. The chemical conjugation approach leads to much lower
400 antimicrobial activities, regardless of the type of functionalized mesoporous silica nanoparticles,
401 whereas the physical adsorption of nisin onto negatively charged mesoporous silica nanoparticles
402 retains its antimicrobial activity. From the results obtained in the loading and release tests, it can
403 be concluded that electrostatic interactions have a crucial role in the mechanism of interaction
404 between nisin and the functional groups existing on the surface of mesoporous silica

405 nanoparticles, and consequently, have an enormous impact on the loading capacity and nisin's
406 release profiles from MSNs-formulated samples. These interactions also affect the antimicrobial
407 activity of nisin loaded onto bare or carboxylated MSNs. The stronger electrostatic interactions
408 between the nisin molecules and carboxyl groups of the carboxyl-functionalized mesoporous
409 silica nanoparticles appear to be responsible for the lower antimicrobial activity of these samples
410 relative to those of the free nisin and nisin loaded onto bare mesoporous silica nanoparticles.
411 This is reflected in the poor release profiles and limited bioavailability of the nisin loaded onto
412 carboxyl-functionalized MSNs in culture medium at neutral pH. In contrast, the stability of nisin
413 loaded onto MSNs was enhanced remarkably overextended preservation times.

414 In comparison with acidic foods, alkaline foods include a wide range of nutrients, which have
415 significant health benefits [42]. In alkaline media, nisin is very unstable and loses its antimicrobial
416 activity. However, its loading onto negatively charged MSNs (bare and carboxylated MSNs)
417 interestingly led to retained antimicrobial activities at pH 9.5. The results from the cytotoxicity
418 tests involving the MTT assay revealed that neither nisin nor nisin-loaded MSNs have any
419 significant toxic effects on the mouse fibroblast L929 cells.

420 In conclusion, the results obtained in this study recommend MSNs as suitable carriers for
421 loading nisin. Furthermore, the applied loading approach is decisive, as it has a great impact on
422 the antimicrobial properties of the loaded nisin. The as-prepared system can be employed in
423 novel controlled release packaging materials. Indeed, polymeric materials used in food
424 packaging can be embedded with nisin-loaded mesoporous silica nanoparticles. The stability and
425 antimicrobial properties of such packaging materials are needed to be comprehensively
426 investigated.

Acknowledgments

This work was financially supported by the National Institute of Genetic Engineering and Biotechnology (NIGEB). The authors thank the NTNU Nanolab for providing instrumentation facilities. The Research Council of Norway is acknowledged for their support of the Norwegian Micro-and Nano-Fabrication Facility, NorFab (197411/V30).

Conflict of interest

The authors declare no competing financial interest.

References

(1) Gálvez, A.; Abriouel, H.; López, R. L.; Omar, N. Ben. *Int. J. Food Microbiol.* **2007**, *120* (1–2), 51–70.

(2) Holley, R. A.; Patel, D. *Food Microbiol.* **2005**, *22* (4), 273–292.

(3) Delves-Broughton, J. *Int. J. Dairy Technol.* **1990**, *43* (3), 73–76.

(4) Thomas, L.; Clarkson, M.; Delves-Broughton, J. In *Natural Food Antimicrobial Systems*; CRC Press: Florida, 2000; pp 463–524.

(5) Prince, A.; Sandhu, P.; Kumar, P.; Dash, E.; Sharma, S.; Arakha, M.; Jha, S.; Akhter, Y.; Saleem, M. *Sci. Rep.* **2016**, *6*, 37908.

(6) Wiedemann, I.; Benz, R.; Sahl, H.-G. *J. Bacteriol.* **2004**, *186* (10), 3259–3261.

(7) Wiedemann, I.; Breukink, E.; van Kraaij, C.; Kuipers, O. P.; Bierbaum, G.; de Kruijff, B.;

446 Sahl, H. G. *J. Biol. Chem.* **2001**, *276* (3), 1772–1779.

447 (8) Abee, T.; Delves-Broughton, J. In *Food Preservatives*; Springer US: Boston, MA, 2003;
448 pp 146–178.

449 (9) Guilhelmelli, F.; Vilela, N.; Albuquerque, P.; Derengowski, L. da S.; Silva-Pereira, I.;
450 Kyaw, C. M. *Front. Microbiol.* **2013**, *4*, 353.

451 (10) Gänzle, M. *Int. J. Food Microbiol.* **1999**, *46* (3), 207–217.

452 (11) Delves-Broughton, J.; Blackburn, P.; Evans, R. J.; Hugenholtz, J. *Antonie Van*
453 *Leeuwenhoek* **1996**, *69* (2), 193–202.

454 (12) Tong, Z.; Zhang, Y.; Ling, J.; Ma, J.; Huang, L.; Zhang, L. *PLoS One* **2014**, *9* (2), e89209.

455 (13) Fahim, H. A.; Khairalla, A. S.; El-Gendy, A. O. *Front. Microbiol.* **2016**, *7*, 1385.

456 (14) Trujillo, L. E.; Ávalos, R.; Granda, S.; Santiago Guerra, L.; País-Chanfrau, J. M. **2016**, *8*
457 (3), 1.

458 (15) Khan, I.; Oh, D.-H. *Innov. Food Sci. Emerg. Technol.* **2016**, *34*, 376–384.

459 (16) Xiao, D.; Davidson, P. M.; Zhong, Q. *J. Agric. Food Chem.* **2011**, *59* (13), 7393–7404.

460 (17) Zohri, M.; Alavidjeh, M. S.; Haririan, I.; Ardestani, M. S.; Ebrahimi, S. E. S.; Sani, H. T.;
461 Sadjadi, S. K. *Probiotics Antimicrob. Proteins* **2010**, *2* (4), 258–266.

462 (18) Krivorotova, T.; Cirkovas, A.; Maciulyte, S.; Staneviciene, R.; Budriene, S.; Serviene, E.;
463 Sereikaite, J. *Food Hydrocoll.* **2016**, *54*, 49–56.

464 (19) Wu, C.; Wu, T.; Fang, Z.; Zheng, J.; Xu, S.; Chen, S.; Hu, Y.; Ye, X.; Ziener, U.;

Landfester, K.; Crespy, D. *RSC Adv.* **2016**, *6* (52), 46686–46695.

(20) Sarkar, P.; Bhunia, A. K.; Yao, Y. *Food Chem.* **2017**, *217*, 155–162.

(21) Sarkar, P.; Bhunia, A.; Yao, Y. *Food Biophys.* **2016**, *11* (4), 311–318.

(22) Hoffmann, F.; Cornelius, M.; Morell, J.; Fröba, M. *Angew. Chemie Int. Ed.* **2006**, *45* (20), 3216–3251.

(23) Slowing, I.; Viveroescoto, J.; Wu, C.; Lin, V. *Adv. Drug Deliv. Rev.* **2008**, *60* (11), 1278–1288.

(24) Balaure, P. C.; Popa, R. A.; Grumezescu, A. M.; Voicu, G.; Rădulescu, M.; Mogoantă, L.; Bălşeanu, T.-A.; Mogoşanu, G. D.; Chifiriuc, M. C.; Bleotu, C.; Holban, A. M.; Bolocan, A. *Int. J. Pharm.* **2016**, *510* (2), 532–542.

(25) Li, L.; Wang, H. *Adv. Healthc. Mater.* **2013**, *2* (10), 1351–1360.

(26) Kruk, M.; Jaroniec, M.; Sakamoto, Y.; Osamu Terasaki; Ryoo, R.; Ko, C. H. *J. Phys. Chem. B* **2000**, *104* (2), 292–301.

(27) Gounani, Z.; Asadollahi, M. A.; Meyer, R. L.; Arpanaei, A. *Int. J. Pharm.* **2018**, *537* (1–2), 148–161.

(28) González, B.; Colilla, M.; Díez, J.; Pedraza, D.; Guembe, M.; Izquierdo-Barba, I.; Vallet-Regí, M. *Acta Biomater.* **2018**.

(29) Bharti, C.; Gulati, N.; Nagaich, U.; Pal, A. *Int. J. Pharm. Investig.* **2015**, *5* (3), 124.

(30) Taebnia, N.; Morshedi, D.; Doostkam, M.; Yaghmaei, S.; Aliakbari, F.; Singh, G.;

484 Arpanaei, A. *RSC Adv.* **2015**, *5* (75), 60966–60974.

485 (31) Sips, R. *J. Chem. Phys.* **1950**, *18* (8), 1024–1026.

486 (32) Sips, R. *J. Chem. Phys* **1948**, *16* (429), 490–495.

487 (33) Siepmann, J.; Peppas, N. A. *Adv. Drug Deliv. Rev.* **2012**, *64*, 163–174.

488 (34) Ritger, P. L.; Peppas, N. A. *J. Control. Release* **1987**, *5* (1), 37–42.

489 (35) Taebnia, N.; Morshedi, D.; Yaghmaei, S.; Aliakbari, F.; Rahimi, F.; Arpanaei, A.
490 *Langmuir* **2016**, *32* (50), 13394–13402.

491 (36) An, Y.; Chen, M.; Xue, Q.; Liu, W. *J. Colloid Interface Sci.* **2007**, *311* (2), 507–513.

492 (37) Liberman, A.; Mendez, N.; Trogler, W. C.; Kummel, A. C. *Surf. Sci. Rep.* **2014**, *69* (2–3),
493 132–158.

494 (38) de Oliveira, L. F.; Bouchmella, K.; Gonçalves, K. de A.; Bettini, J.; Kobarg, J.; Cardoso,
495 M. B. *Langmuir* **2016**, *32* (13), 3217–3225.

496 (39) Bi, L.; Yang, L.; Narsimhan, G.; Bhunia, A. K.; Yao, Y. *J. Control. Release* **2011**, *150*
497 (2), 150–156.

498 (40) Prombutara, P.; Kulwatthanasal, Y.; Supaka, N.; Sramala, I.; Chareonpornwattana, S.
499 *Food Control* **2012**, *24* (1–2), 184–190.

500 (41) Zou, Y.; Lee, H.-Y.; Seo, Y.-C.; Ahn, J. *J. Food Sci.* **2012**, *77* (3), M165–M170.

501 (42) Schwalfenberg, G. K. *J. Environ. Public Health* **2012**, *2012*, 727630.

502

Figure Captions

Fig. 1 STEM (a) and bright field STEM (b) images, and size distribution curve (c) of the as-prepared BMSNs

Scheme. 1 A schematic illustration of the approaches applied to loading nisin onto MSNs with various types of surface chemistries, either through electrostatic interactions with negatively charged nanoparticles, *i.e.*, BMSNs and CMSNs, or covalent conjugation to amine-functionalized, PEI-coated or carboxyl-functionalized MSNs, *i.e.*, AMSNs, PAMSNs and CMSNs. The insets show the TEM images of the as-prepared MSNs

Fig. 2 Nisin adsorption isotherms and corresponding fitted Langmuir, Freundlich and Langmuir-Freundlich models (a and c), and nisin loading efficiencies (b and d) for BMSNs and CMSNs, respectively, obtained for 200 μg of nanoparticles in 750 μL of acetate buffer at room temperature

Fig. 3 The effect of initial nisin concentration on the Loading capacity (a) and loading efficiency (b) of nisin conjugated to 200 μg of CMSNs, AMSNs and PAMSNs in 750 μL of acetate buffer, pH 5.5, at room temperature

Fig. 4 Loading capacity (a) and loading efficiency (b) of nisin adsorbed onto BMSNs or CMSNs (nisin+BMSNs and nisin+CMSNs, respectively) and nisin conjugated to CMSNs or AMSNs (nisin-AMSNs and nisin-CMSNs, respectively) as determined by the HPLC technique using the nisin and MSNs initial concentrations of 200 μg in 750 μL of acetate buffer, pH 5.5

Fig. 5 The release profiles of nisin from nisin+BMSNs and nisin+CMSNs samples in acetate (pH 5.5), phosphate (pH 7.5) and Tris (pH 9.5) buffers at 37 °C. Both types of the nisin-loaded

524 samples were obtained by loading 200 μg of nisin onto 200 μg of MSNs in 750 μL of acetate
525 buffer

526 **Fig. 6** Desorption kinetics data of nisin from nisin+BMSNs and nisin+CMSNs in acetate (a,d),
527 phosphate (b,e) and Tris (c,f) buffers, respectively, at 37 °C; and the corresponding zero order
528 (- - -), first order (.....) and the power-law (⎯⎯) models fits. Both types of the nisin-loaded
529 samples were prepared as mentioned in Fig. 5

530 **Fig. 7** The release profiles of nisin from nisin-conjugated samples (nisin-CMSNs, nisin-AMSNs
531 and nisin-PAMSNs) in phosphate buffer, pH 7.5, at 37 °C. All three samples were obtained by
532 loading 200 μg of nisin onto 200 μg of MSNs in 750 μL of acetate buffer, pH 5.5

533 **Fig. 8** The antimicrobial properties of free nisin and various nisin-loaded MSNs at different
534 concentrations against *Staphylococcus aureus*

535 **Fig. 9** The effect of the preservation time on the antimicrobial activity of free nisin (a),
536 nisin+BMSNs (b) and nisin+CMSNs (c) at different nisin concentrations

537 **Fig. 10** The antimicrobial activity of free nisin, nisin-adsorbed onto BMSNs and CMSNs at pH
538 9.5

539 **Fig. 11** Changes in the cell viability of mouse fibroblast L929 cells following treatment with
540 BMSNs, CMSNs, AMSNs, PAMSNs, nisin (a); nisin-loaded BMSNs and nisin-loaded BCMSNs
541 (b), evaluated at different nisin concentrations using MTT assay

Table 1. The equation's parameters of the Langmuir, Freundlich and Langmuir-Freundlich models for the physical adsorption of nisin onto BMSNs and CMSNs, obtained for 200 μg of nanoparticles in 750 μL of acetate buffer, pH 5.5, at room temperature.

	Langmuir			**Freundlich**			**Langmuir- Freundlich**			
	q_m	K_l	R^2	n	K_F	R^2	K_c	n	q_m	R^2
BMSNs	0.85±0.06	0.03±0.007	0.974	3.02±0.37	1.21±0.12	0.970	5.95±4.81	1.52±0.31	1.09±0.21	0.993
CMSNs	2.24±0.19	0.19±0.03	0.997	1.40±0.12	3.72±0.50	0.986	13.7±4.71	0.84±0.05	1.69±0.14	0.999

Table 2. Release kinetic parameters after fitting nisin-release data to the zero-order, first-order, and the power-law models for BMSNs and CMSNs in acetate (pH 5.5), phosphate (pH 7.5) and Tris (pH 9.5) buffers at 37 °C. Both nisin-loaded samples were obtained by loading 200 μg of nisin onto 200 μg of MSNs in 750 μL of acetate buffer.

		Zero-order		**First-order**		**Power-law**		
		K_0	R^2	K_1	R^2	K	n	R^2
BMSNs	Acetate buffer	0.011±0.002	0.598	0.022±0.004	0.794	0.118±0.011	0.416±0.025	0.988
	Phosphate buffer	0.016±0.003	0.365	0.056±0.014	0.781	0.204±0.018	0.358±0.024	0.982
	Tris buffer	0.015±0.003	-0.68	0.093±0.035	0.280	0.289±0.019	0.253±0.019	0.974
CMSNs	Acetate buffer	0.007±0.001	0.260	0.010±0.002	0.424	0.100±0.006	0.343±0.025	0.980
	Phosphate buffer	0.010±0.002	0.552	0.018±0.003	0.734	0.109±0.019	0.41±0.046	0.961
	Tris buffer	0.016±0.003	0.056	0.102±0.022	0.854	0.248±0.028	0.319±0.032	0.963

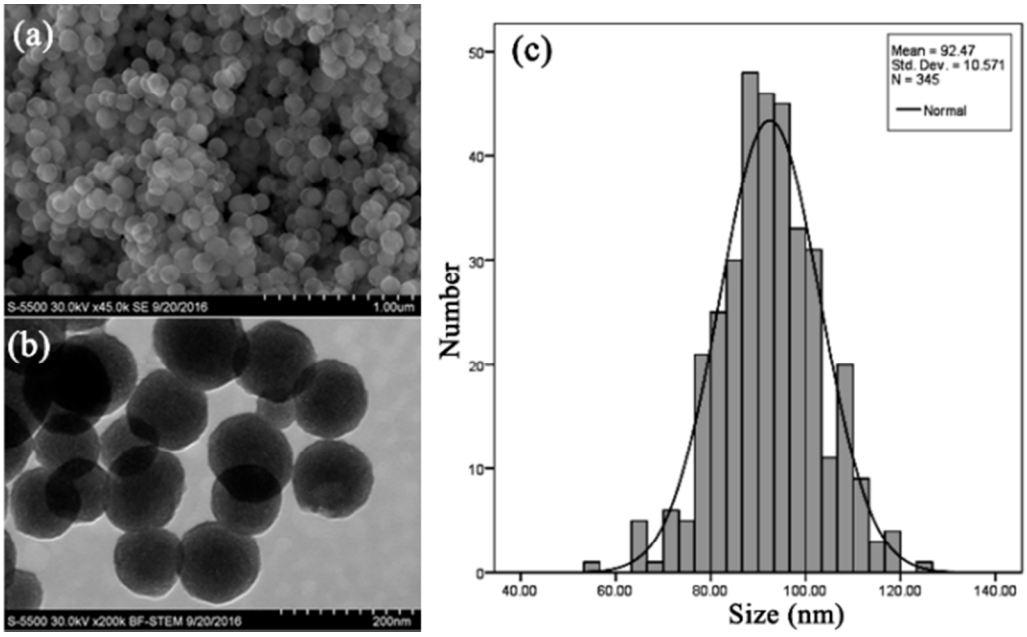
(a)
S-5500 30.0kV x45.0k SE 9/20/2016
1.00um
(b)
S-5500 30.0kV x200k BF-STEM 9/20/2016
200nm
(c)
Mean = 92.47
Std. Dev. = 10.571
N = 345
Normal
Number
Size (nm)
0
10
20
30
40
50
40.00
60.00
80.00
100.00
120.00
140.00

Fig. 1

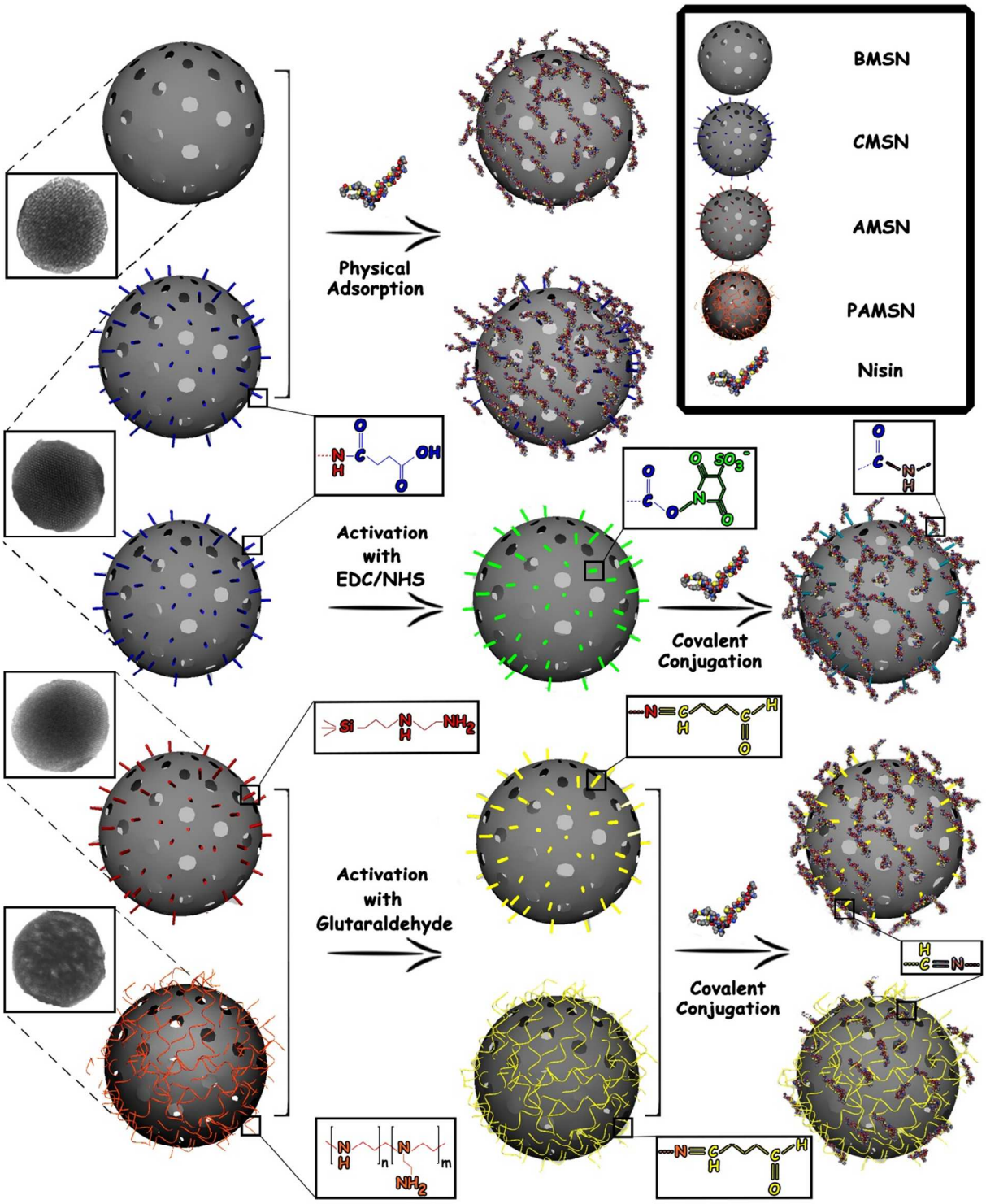
BMSN
CMSN
AMSN
PAMSN
Nisin
Physical Adsorption
Activation with EDC/NHS
Covalent Conjugation
Activation with Glutaraldehyde
Covalent Conjugation

Scheme. 1

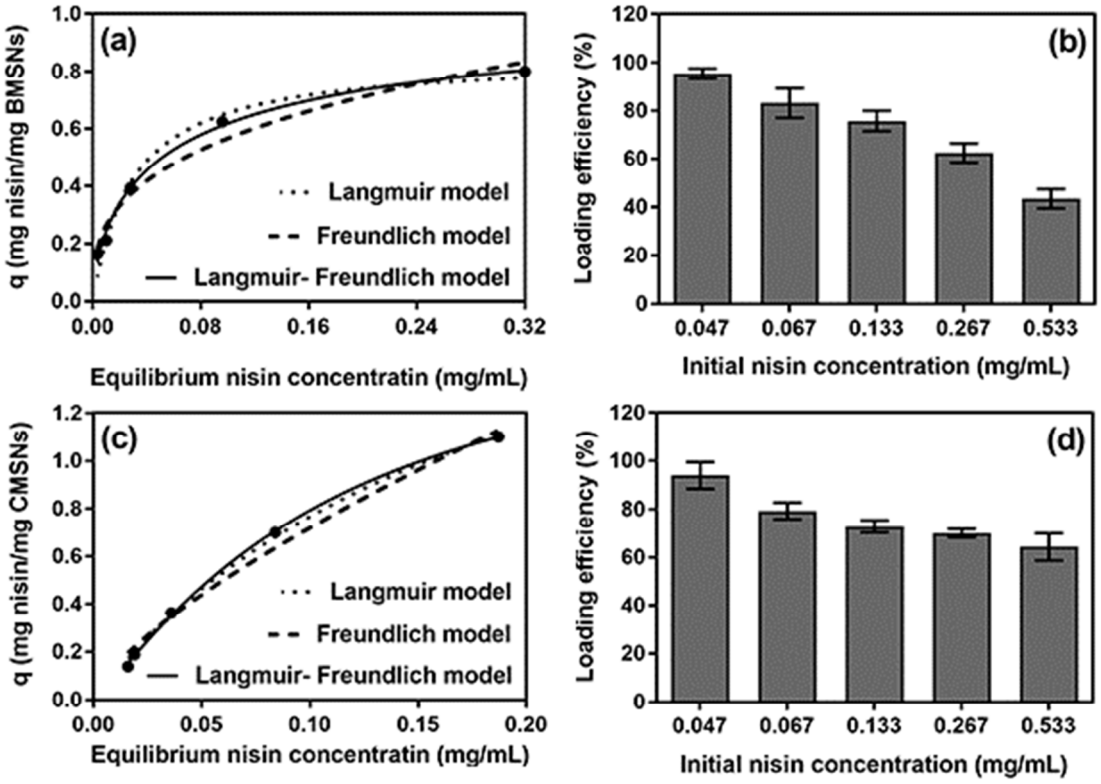
(a)
q (mg nisin/mg BMSNs)
Langmuir model
Freundlich model
Langmuir- Freundlich model
Equilibrium nisin concentratin (mg/mL)
(b)
Loading efficiency (%)
Initial nisin concentration (mg/mL)
(c)
q (mg nisin/mg CMSNs)
Langmuir model
Freundlich model
Langmuir- Freundlich model
Equilibrium nisin concentratin (mg/mL)
(d)
Loading efficiency (%)
Initial nisin concentration (mg/mL)

Fig. 2

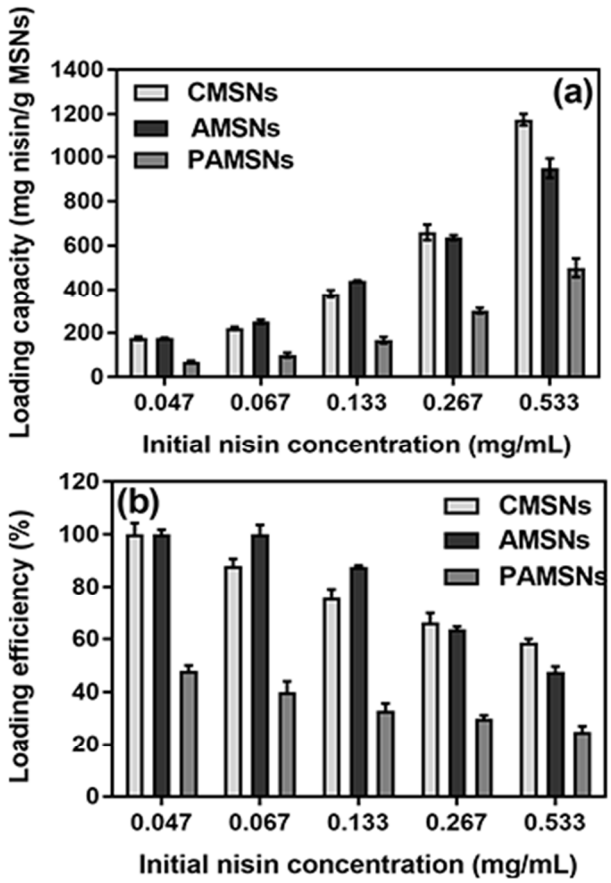
Loading capacity (mg nisin/g MSNs)
1400
1200
1000
800
600
400
200
0
CMSNs
AMSNs
PAMSNs
(a)
0.047
0.067
0.133
0.267
0.533
Initial nisin concentration (mg/mL)
Loading efficiency (%)
120
100
80
60
40
20
0
(b)
CMSNs
AMSNs
PAMSNs
0.047
0.067
0.133
0.267
0.533
Initial nisin concentration (mg/mL)

Fig. 3

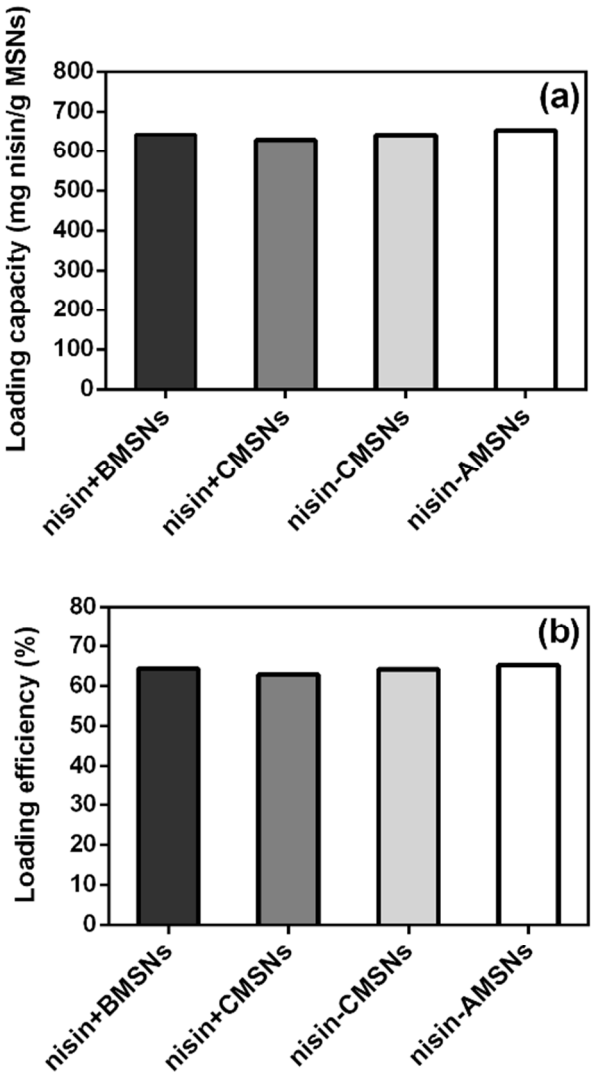
(a)
Loading capacity (mg nisin/g MSNs)
800
700
600
500
400
300
200
100
0
nisin+BMSNs
nisin+CMSNs
nisin-CMSNs
nisin-AMSNs
(b)
Loading efficiency (%)
80
70
60
50
40
30
20
10
0
nisin+BMSNs
nisin+CMSNs
nisin-CMSNs
nisin-AMSNs

Fig. 4

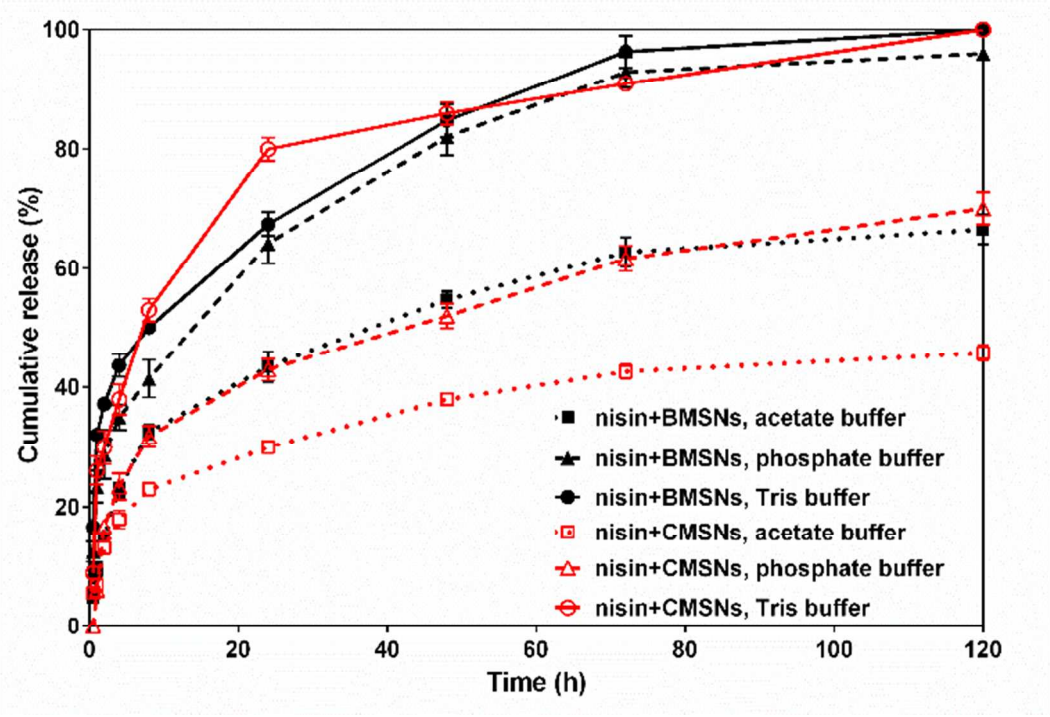
Cumulative release (%)
Time (h)
0
20
40
60
80
100
120
nisin+BMSNs, acetate buffer
nisin+BMSNs, phosphate buffer
nisin+BMSNs, Tris buffer
nisin+CMSNs, acetate buffer
nisin+CMSNs, phosphate buffer
nisin+CMSNs, Tris buffer

Fig. 5

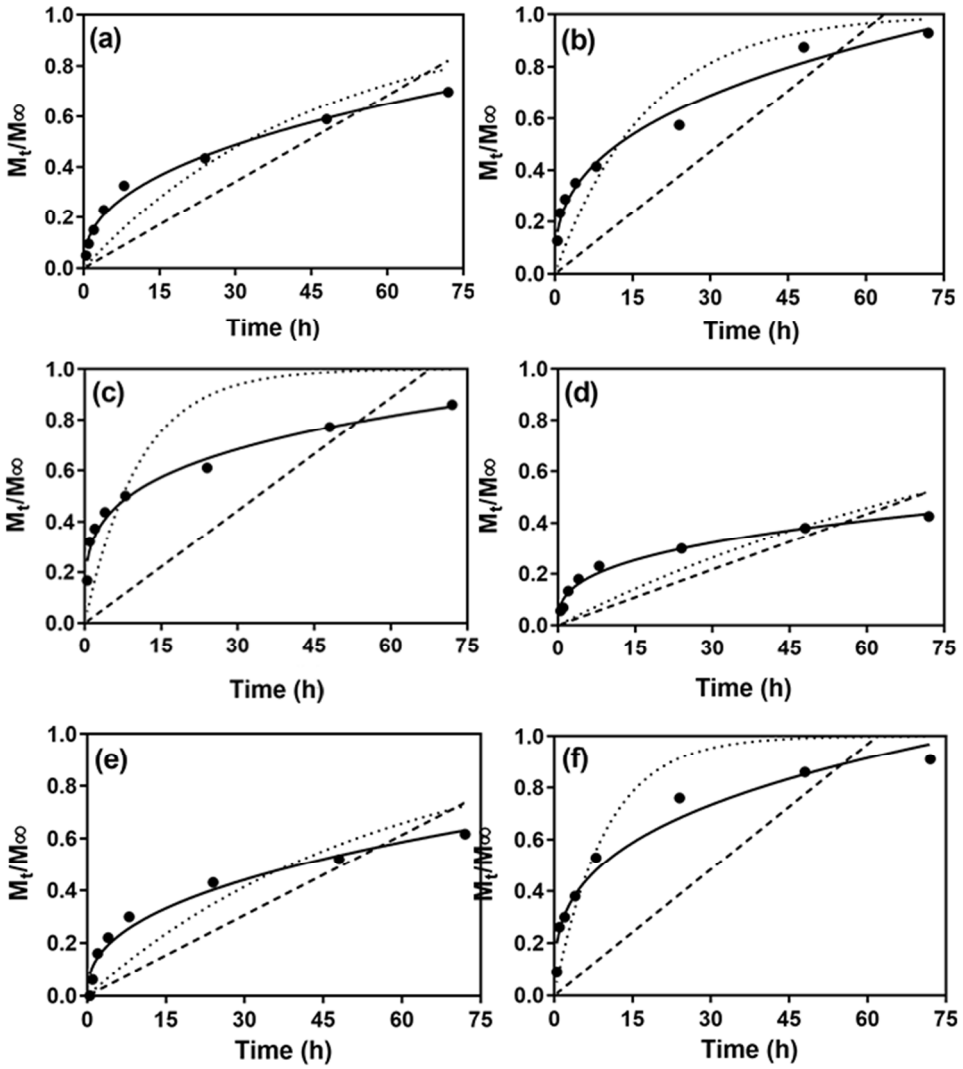

Fig. 6

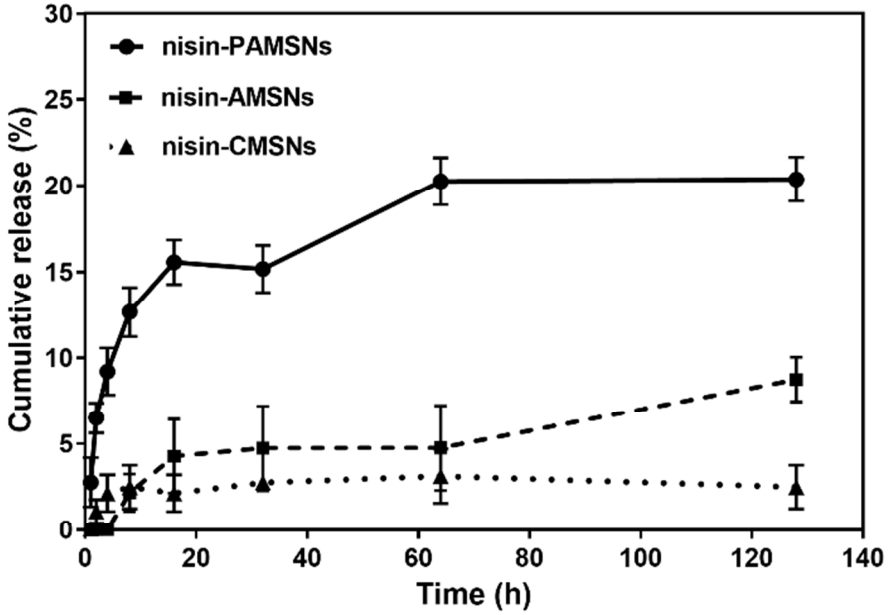
nisin-PAMSNs
nisin-AMSNs
nisin-CMSNs
Cumulative release (%)
Time (h)
0
5
10
15
20
25
30
0
20
40
60
80
100
120
140

Fig. 7

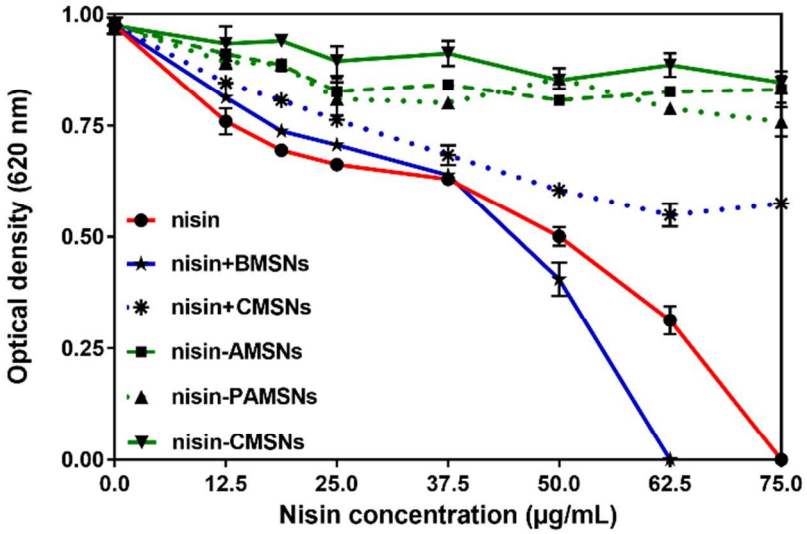
Optical density (620 nm)
1.00
0.75
0.50
0.25
0.00
0.0
12.5
25.0
37.5
50.0
62.5
75.0
Nisin concentration (μg/mL)
nisin
nisin+BMSNs
nisin+CMSNs
nisin-AMSNs
nisin-PAMSNs
nisin-CMSNs

Fig. 8

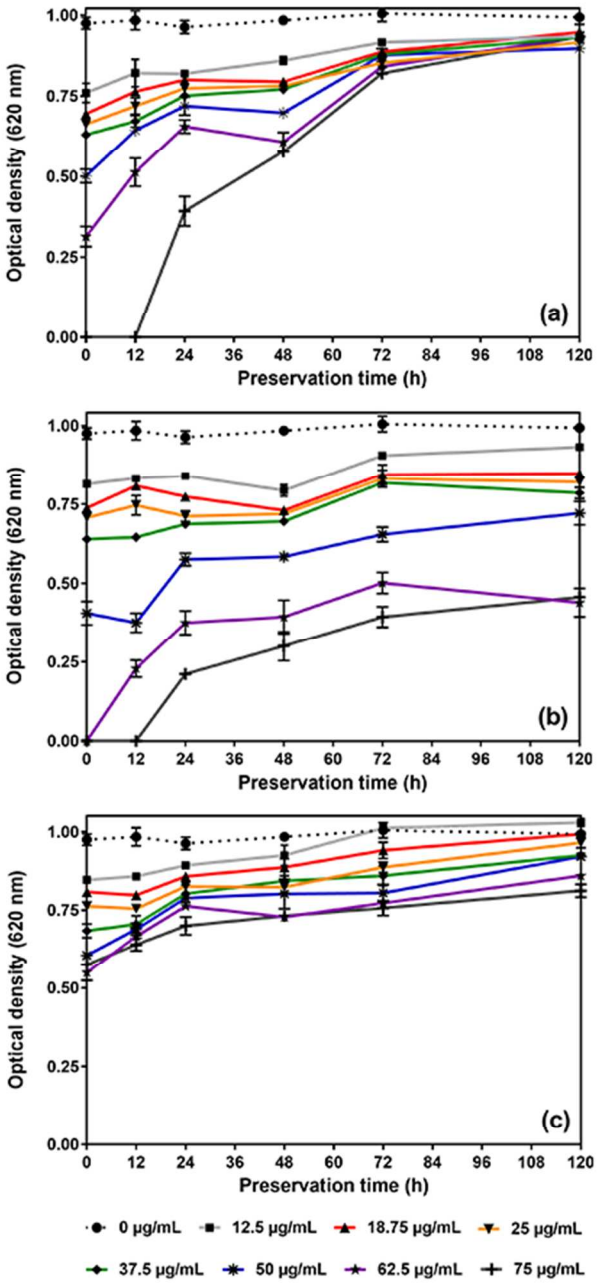
Optical density (620 nm)
Preservation time (h)
(a)
(b)
(c)
0 μg/mL
12.5 μg/mL
18.75 μg/mL
25 μg/mL
37.5 μg/mL
50 μg/mL
62.5 μg/mL
75 μg/mL

Fig. 9

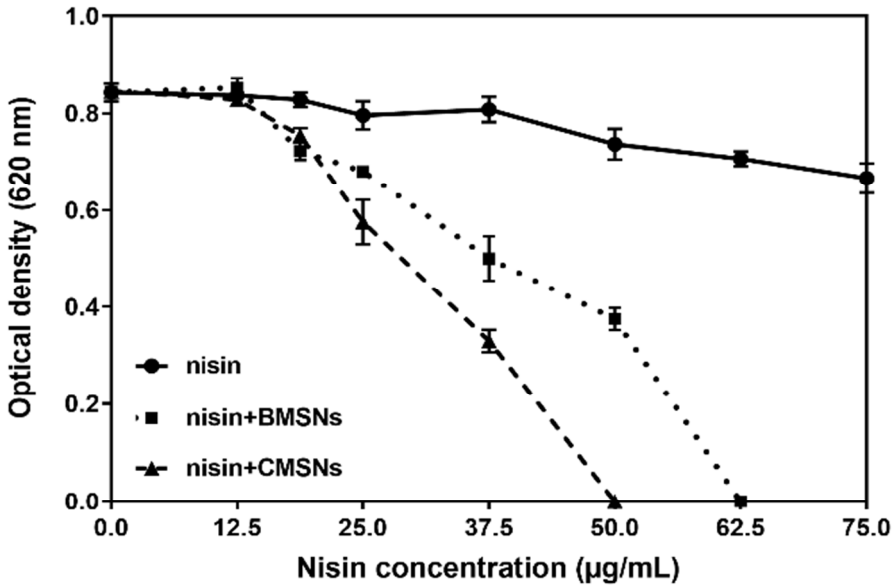
Optical density (620 nm)
1.0
0.8
0.6
0.4
0.2
0.0
nisin
nisin+BMSNs
nisin+CMSNs
0.0
12.5
25.0
37.5
50.0
62.5
75.0
Nisin concentration (μg/mL)

Fig. 10

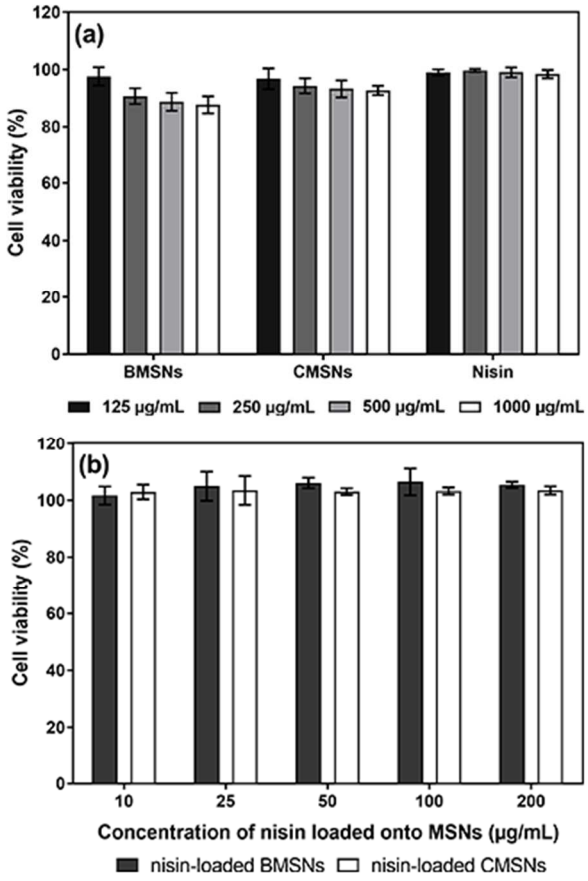
(a)
Cell viability (%)
120
100
80
60
40
20
0
BMSNs
CMSNs
Nisin
125 μg/mL
250 μg/mL
500 μg/mL
1000 μg/mL
(b)
Cell viability (%)
10
25
50
100
200
Concentration of nisin loaded onto MSNs (μg/mL)
nisin-loaded BMSNs
nisin-loaded CMSNs

Fig. 11

"TOC Graphic"

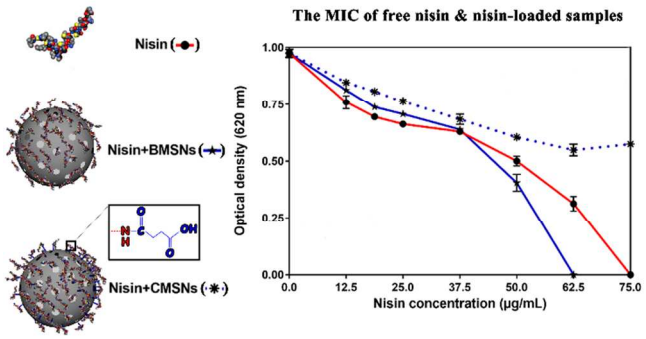
Nisin (-●-)
Nisin+BMSNs (-★-)
Nisin+CMSNs (-✱-)
The MIC of free nisin & nisin-loaded samples
Optical density (620 nm)
1.00
0.75
0.50
0.25
0.00
0.0
12.5
25.0
37.5
50.0
62.5
75.0
Nisin concentration (μg/mL)

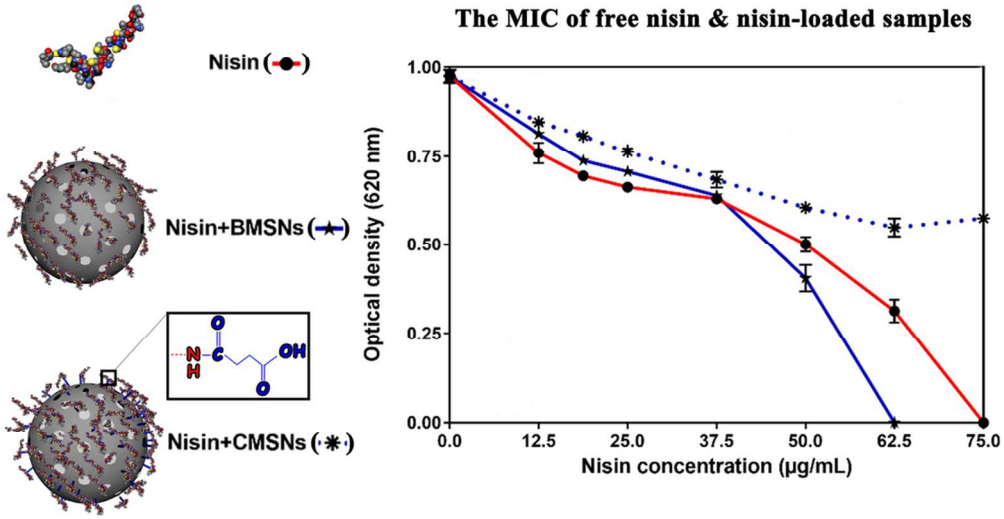

TOC Graphic

47x26mm (600 x 600 DPI)

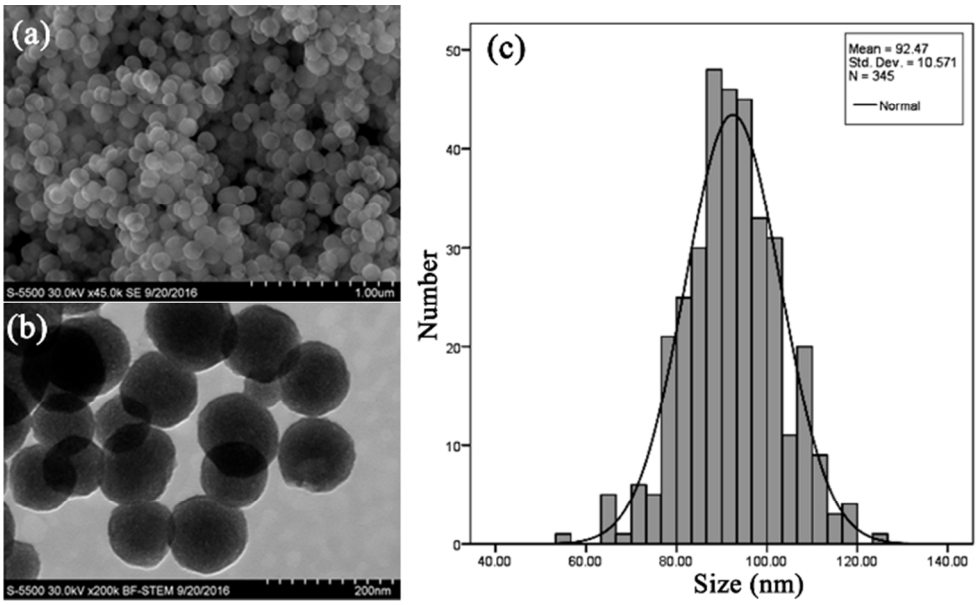

Figure. 1. STEM (a) and bright field STEM (b) images, and size distribution curve (c) of the as-prepared BMSNs.

87x52mm (220 x 220 DPI)

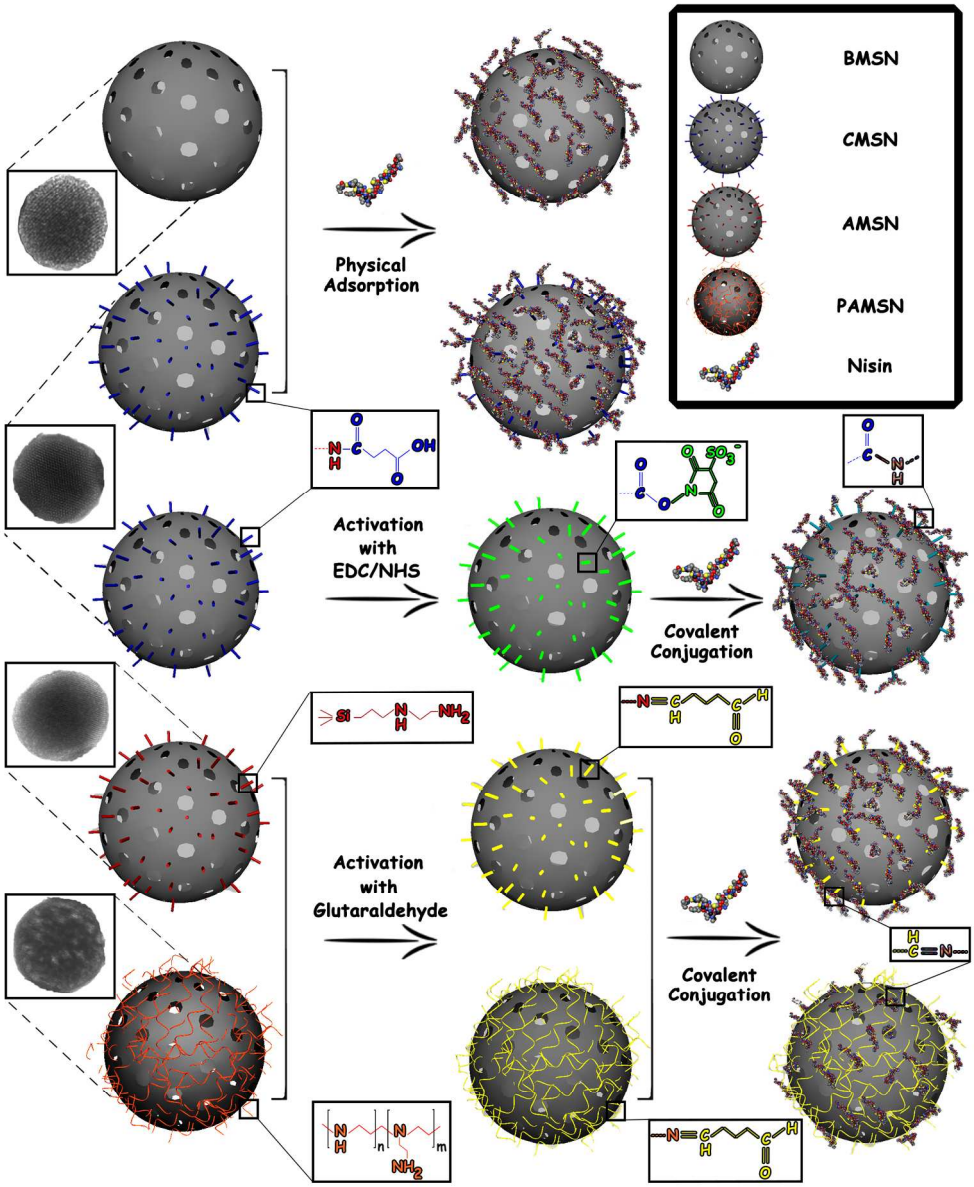

Scheme. 1. A schematic illustration of the approaches applied to loading nisin onto MSNs with various types of surface chemistries, either through electrostatic interactions with negatively charged nanoparticles, i.e., BMSNs and CMSNs, or covalent conjugation to amine-functionalized, PEI-coated or carboxyl-functionalized MSNs, i.e., AMSNs, PAMSNs and CMSNs. The insets show the TEM images of the as-prepared MSNs.

767x917mm (72 x 72 DPI)

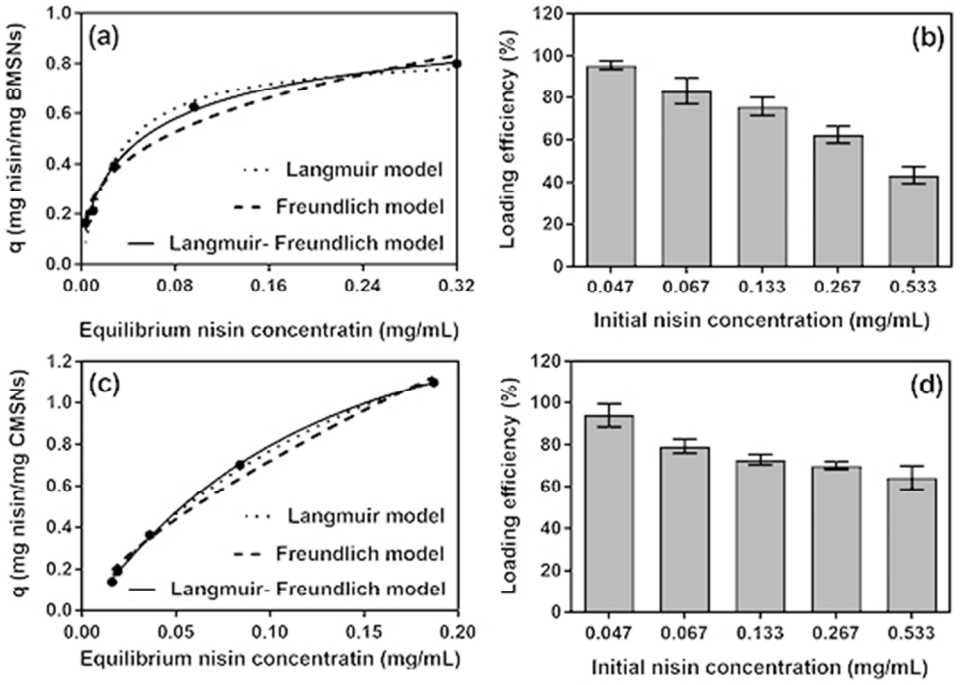

Figure 2. Nisin adsorption isotherms and corresponding fitted Langmuir, Freundlich and Langmuir-Freundlich models (a and c), and nisin loading efficiencies (b and d) for BMSNs and CMSNs, respectively, obtained for 200 µg of nanoparticles in 750 µL of acetate buffer at room temperature.

211x148mm (72 x 72 DPI)

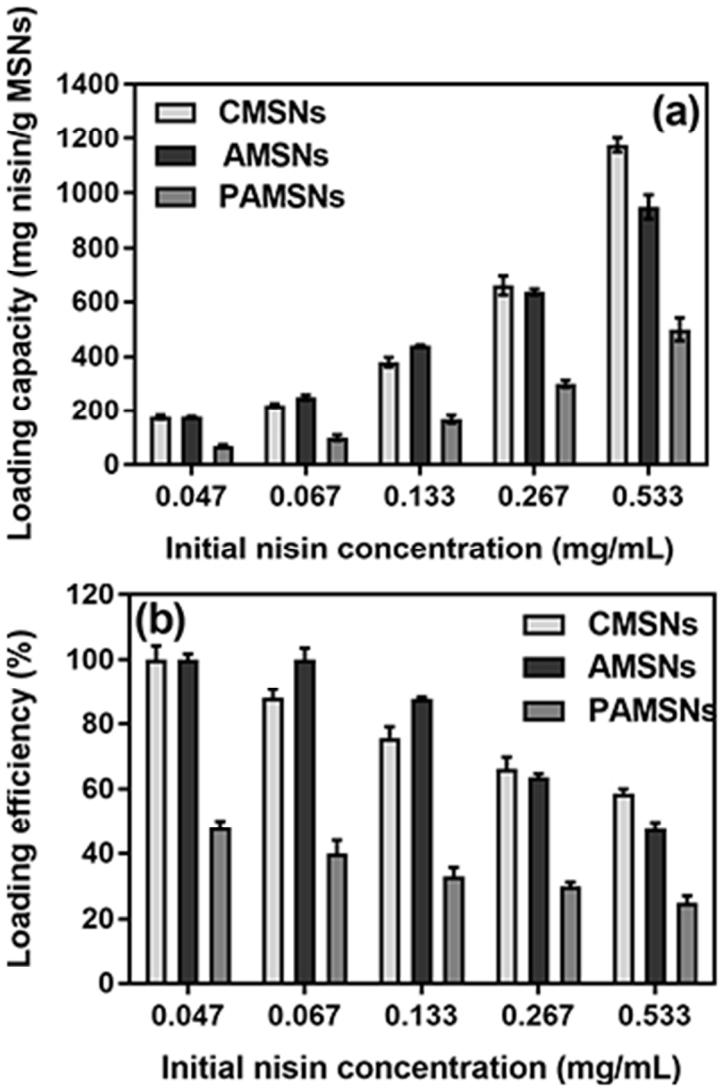

Figure 3. The effect of initial nisin concentration on the Loading capacity (a) and loading efficiency (b) of nisin conjugated to 200 µg of CMSNs, AMSNs and PAMSNs in 750 µL of acetate buffer, pH 5.5, at room temperature.

133x196mm (72 x 72 DPI)

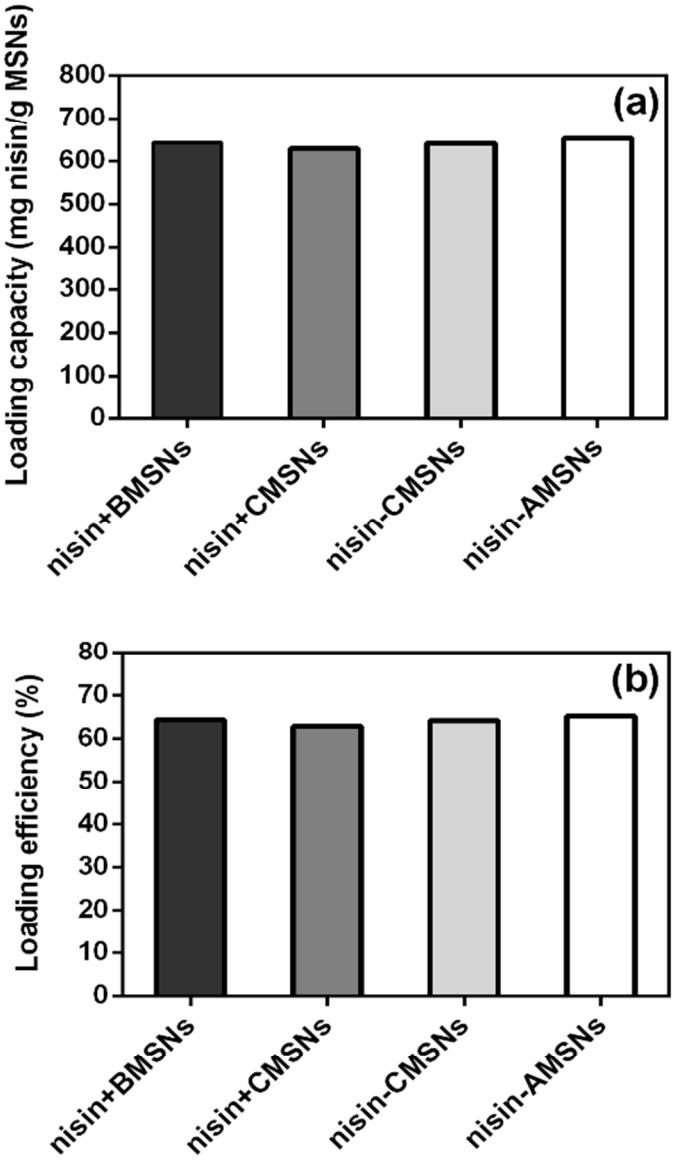

Figure 4. Loading capacity (a) and loading efficiency (b) of nisin adsorbed onto BMSNs or CMSNs (nisin+BMSNs and nisin+CMSNs, respectively) and nisin conjugated to CMSNs or AMSNs (nisin-AMSNs and nisin-CMSNs, respectively) as determined by the HPLC technique using the nisin and MSNs initial concentrations of 200 µg in 750 µL of acetate buffer, pH 5.5.

66x110mm (220 x 220 DPI)

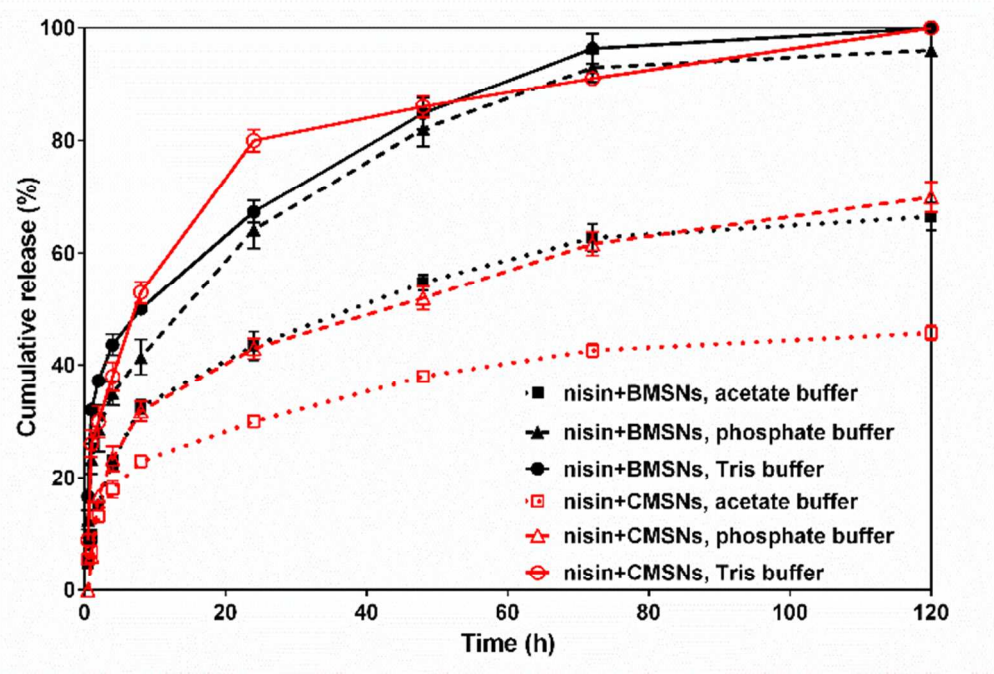

Figure 5. The release profiles of nisin from nisin+BMSNs and nisin+CMSNs samples in acetate (pH 5.5), phosphate (pH 7.5) and Tris (pH 9.5) buffers at 37 °C. Both types of the nisin-loaded samples were obtained by loading 200 µg of nisin onto 200 µg of MSNs in 750 µL of acetate buffer.

88x60mm (220 x 220 DPI)

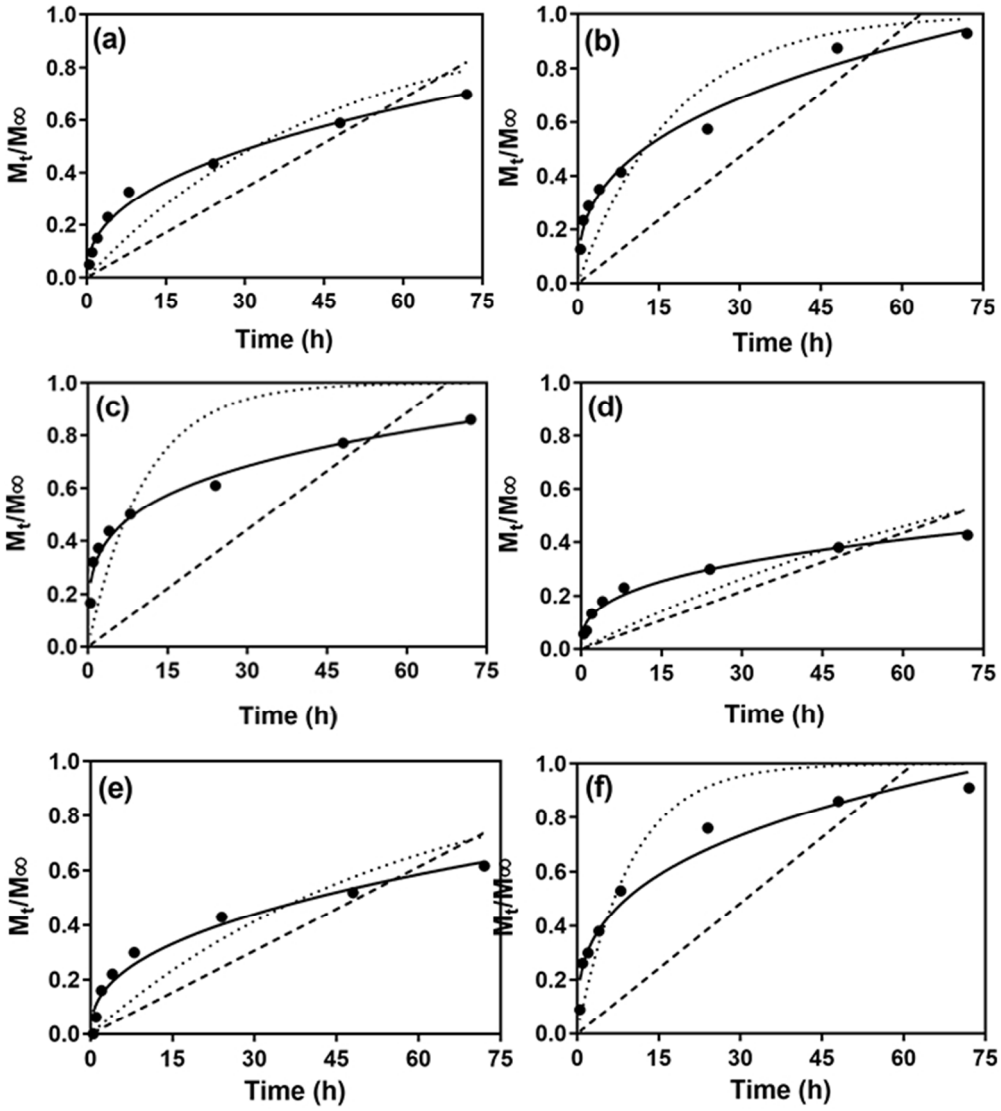

Figure 6. Desorption kinetics data of nisin from nisin+BMSNs and nisin+CMSNs in acetate (a,d), phosphate (b,e) and Tris (c,f) buffers, respectively, at 37 °C; and the corresponding zero order (- - -), first order (.....) and the power-law (___) models fits. Both types of the nisin-loaded samples were prepared as mentioned in Figure. 5.

258x291mm (72 x 72 DPI)

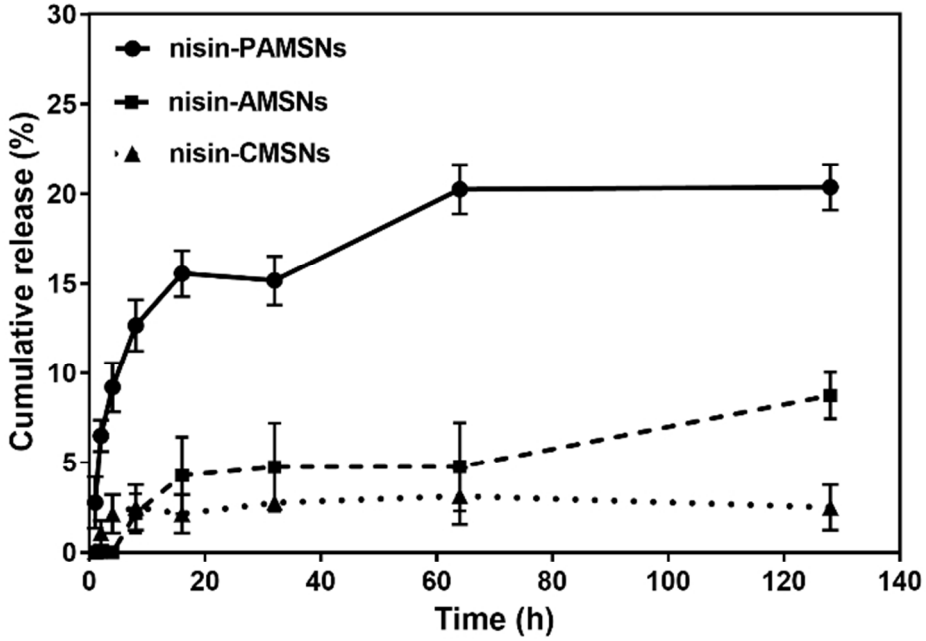

Figure 7. The release profiles of nisin from nisin-conjugated samples (nisin-CMSNs, nisin-AMSNs and nisin-PAMSNs) in phosphate buffer, pH 7.5, at 37 °C. All three samples were obtained by loading 200 µg of nisin onto 200 µg of MSNs in 750 µL of acetate buffer, pH 5.5.

88x60mm (220 x 220 DPI)

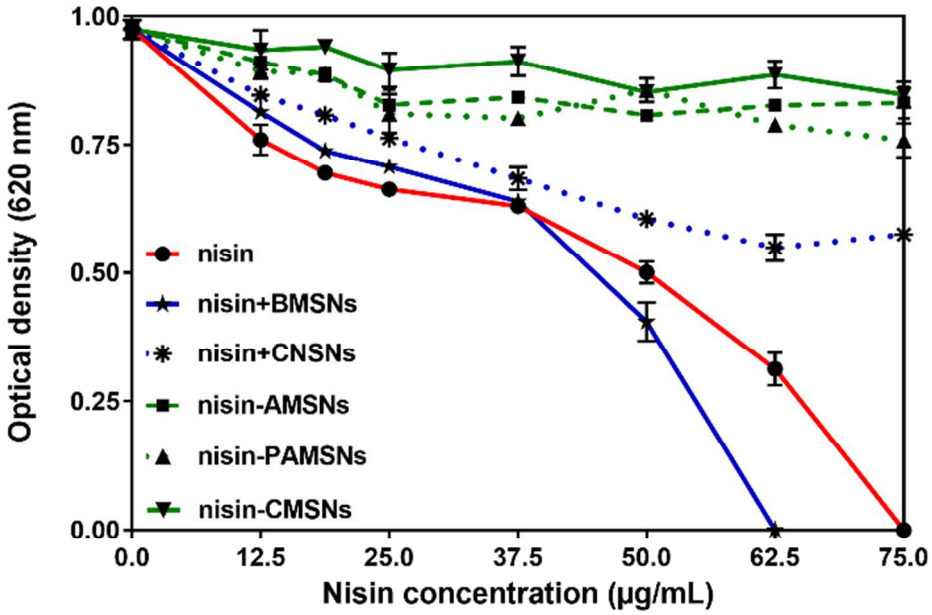

Figure 8. The antimicrobial properties of free nisin and various nisin-loaded MSNs at different concentrations against Staphylococcus aureus.

87x58mm (220 x 220 DPI)

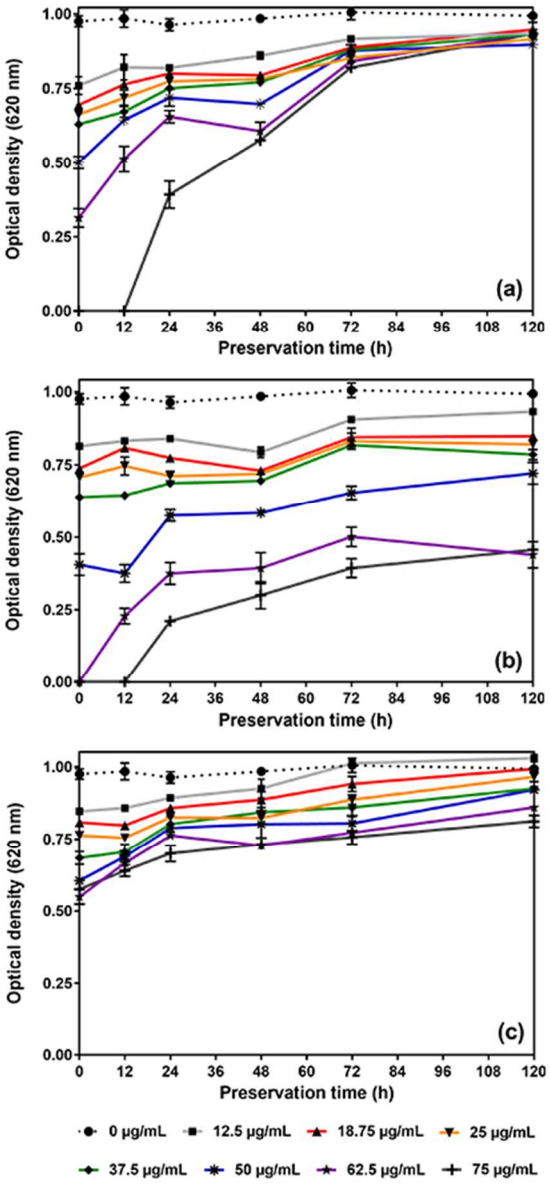

Figure 9. The effect of the preservation time on the antimicrobial activity of free nisin (a), nisin+BMSNs (b) and nisin+CMSNs (c) at different nisin concentrations.

155x317mm (72 x 72 DPI)

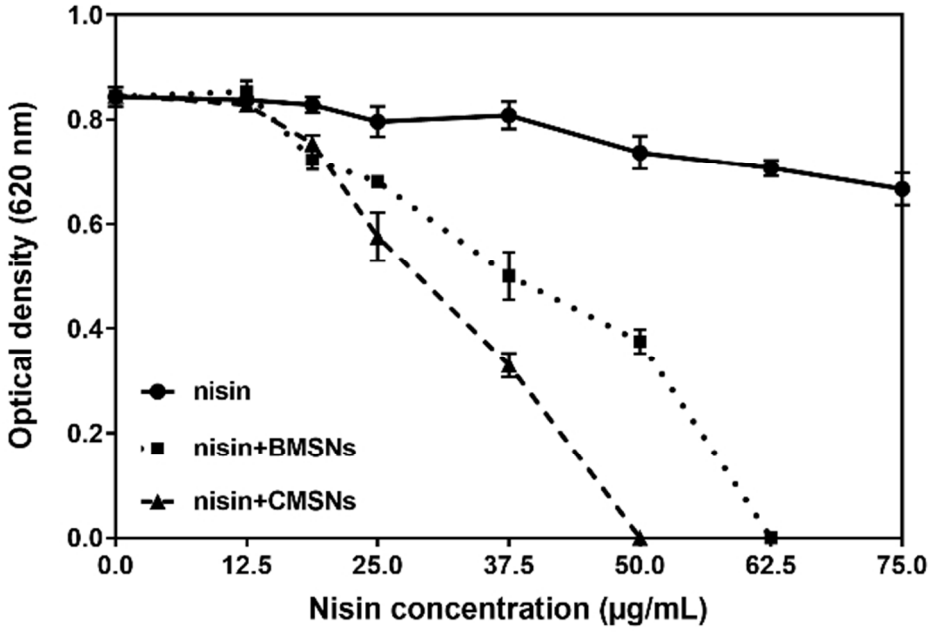

Figure 10. The antimicrobial activity of free nisin, nisin-adsorbed onto BMSNs and CMSNs at pH 9.5.

81x55mm (220 x 220 DPI)

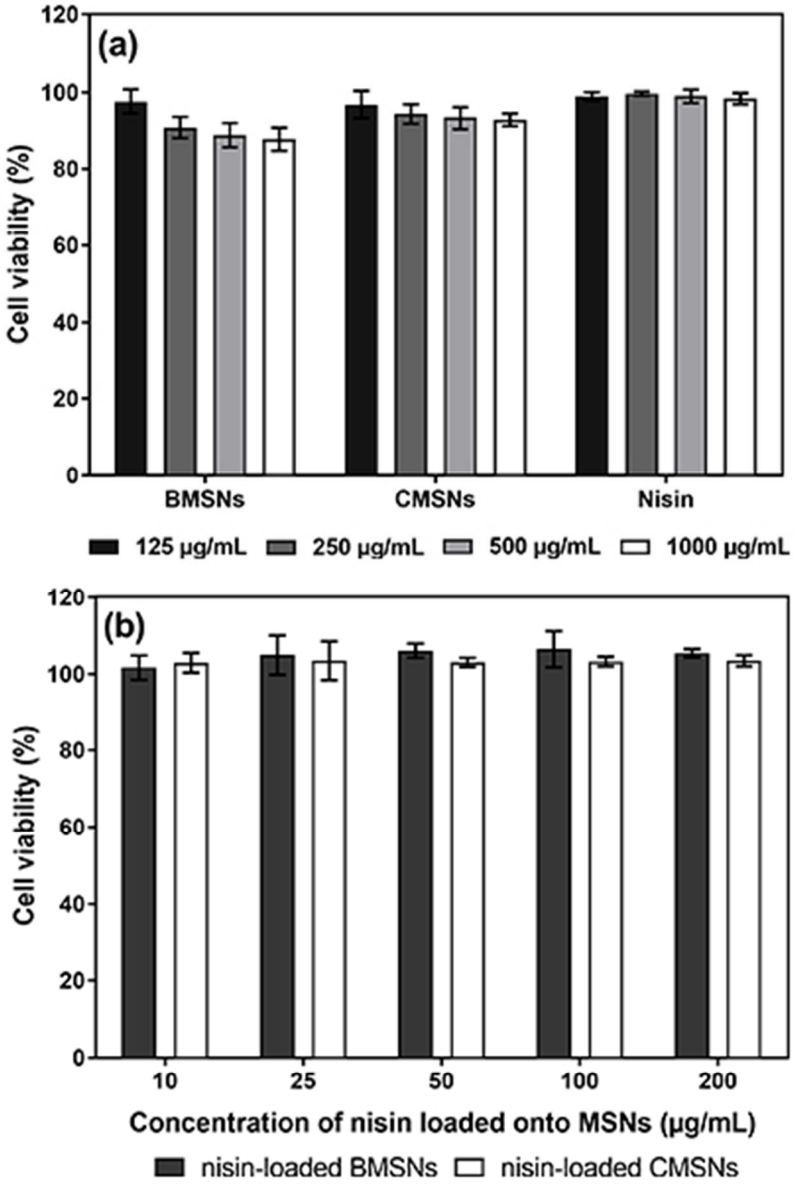

Figure 11. Changes in the cell viability of mouse fibroblast L929 cells following treatment with BMSNs, CMSNs, AMSNs, PAMSNs, nisin (a); nisin-loaded BMSNs and nisin-loaded BCMSNs (b), evaluated at different nisin concentrations using MTT assay.

155x215mm (72 x 72 DPI)